Band structure engineering and non-equilibrium dynamics in Floquet topological insulators

Mark S. Rudner[1] ✉ *and Netanel H. Lindner*[2]

Abstract | Non-equilibrium topological phenomena can be induced in quantum many-body systems using time-periodic fields (for example, by laser or microwave illumination). This Review begins with the key principles underlying Floquet band engineering, wherein such fields are used to change the topological properties of a system's single-particle spectrum. In contrast to equilibrium systems, non-trivial band structure topology in a driven many-body system does not guarantee that robust topological behaviour will be observed. In particular, periodically driven many-body systems tend to absorb energy from their driving fields and thereby tend to heat up. We survey various strategies for overcoming this challenge of heating and for obtaining new topological phenomena in this non-equilibrium setting. We describe how drive-induced topological edge states can be probed in the regime of mesoscopic transport, and three routes for observing topological phenomena beyond the mesoscopic regime: long-lived transient dynamics and prethermalization, disorder-induced many-body localization, and engineered couplings to external baths. We discuss the types of phenomena that can be explored in each of the regimes covered, and their experimental realizations in solid-state, cold atomic, and photonic systems.

Recently developed experimental tools for probing and controlling quantum systems provide access to quantum many-body dynamics on time and length scales, and with levels of precision, that were nearly unimaginable just a few decades ago. In addition to enabling deep new insights into the properties of quantum materials, these tools allow us to explore fundamentally new regimes of quantum many-body dynamics. On a practical level, laser and microwave driving fields also open the possibility of dynamically controlling and modifying quantum material properties 'on demand'[1].

As briefly outlined below, Floquet theory[2] provides a powerful framework for analysing periodically driven quantum systems; for this reason, the names 'periodically driven systems' and 'Floquet systems' are used interchangeably. Of particular interest for this Review, periodic driving provides means to manipulate the dispersion and geometry of (Floquet)–Bloch bands in atomic[3–5] or electronic[6] systems with periodic lattice potentials. Inspired by the recent discovery of topological insulators (TIs)[7], a series of early works developed the notion of a 'Floquet topological insulator' (FTI): by appropriately choosing the drive frequency, amplitude and symmetry, periodic driving can be used to change the topological features of a system's Bloch bands[8–10].

Crucially, while a periodic drive may be used to induce a topologically non-trivial Floquet band structure for electrons or cold atoms, this is not enough to ensure that the system displays physical properties that one might expect or hope to produce by analogy with equilibrium TIs. The Floquet bands provide the stage on which the system's dynamics play out; the physical properties of the system are determined by the many-body state that is obtained. In particular, realizing behaviour akin to that of an equilibrium TI requires obtaining a many-body state that resembles that of a conventional band insulator (which is characterized by having all bands either completely filled or empty). Finding the conditions in which a periodically driven system can host a stable stationary (or nearly stationary) state with non-trivial topological characteristics is therefore one of the central challenges in the field.

Importantly, in the absence of coupling to an external environment, it is widely believed that a generic, closed, periodically driven quantum system containing many interacting particles will absorb energy from the driving field and increase its local entropy density, tending towards a featureless state at long times in which all local correlations are fully random (as in an infinite-temperature state)[11,12]. In such a state, no topological

[1]*Niels Bohr International Academy and the Center for Quantum Devices, Niels Bohr Institute, University of Copenhagen, Copenhagen, Denmark.*

[2]*Physics Department, Technion, Haifa, Israel.*

✉*e-mail: rudner@nbi.ku.dk*

https://doi.org/10.1038/s42254-020-0170-z

Key points

- Time-periodic fields provide a versatile platform for inducing non-equilibrium topological phenomena in quantum systems.
- In contrast to equilibrium systems, non-trivial band structure topology does not guarantee that robust topological behaviour will be observed in a many-body system.
- Various strategies can be employed to obtain novel topological phenomena in this non-equilibrium many-body setting.
- Driving-induced topological edge states can be revealed through (non-quantized) mesoscopic transport.
- Working in regimes where heating rates are strongly suppressed allows robust topological behaviour to be observed in long-lived transients.
- Many-body localization due to strong disorder provides a mechanism for completely eliminating heating in certain types of systems, allowing a sharp delineation of intrinsic phases of many-body Floquet systems.
- Bath engineering provides a powerful means for ensuring that the topological properties of a driven system coupled to its natural environment are reflected in its steady state.

phenomena can persist. Therefore, to stabilize non-trivial topological phenomena in Floquet systems, it is necessary to develop strategies to avoid such heating. Exceptions to the runaway heating scenario, for example, based on localization in energy space[13–17] or finite-size effects[18], are also being explored.

A variety of approaches for stabilizing FTIs and other Floquet phases such as Floquet time crystals are being investigated, leveraging regimes of high-or low-frequency driving, disorder-induced localization, and/or bath engineering. In this Review, we outline the main principles underlying these approaches, and some of the key results obtained so far.

Over the past decade, work on Floquet systems has developed in a number of interesting directions, including Floquet engineering of magnetic and other strongly correlated phases[19–23], as well as the formulation of topological classifications[9,24–31] and notions of symmetry-breaking[32–38] and symmetry-protected topological phases in non-equilibrium quantum many-body systems[38–42]. These developments motivated investigations of fundamental questions in non-equilibrium quantum dynamics, including the manifestations of ergodicity and localization, and the dynamics of (pre)thermalization in the unitary evolution of quantum many-body systems, which naturally arise and can be addressed in many-body Floquet systems[43]. Many of these directions have been explored experimentally in cold atoms[44,45], photonics[46] and solid-state systems[47,48]. In this Review, we primarily focus on FTIs and their realization in solid-state, cold atomic and photonic systems.

Our goal in this Review is to provide a pedagogical introduction to key concepts underlying the formation and topological characterization of Floquet–Bloch bands, and their physical manifestations. In illustrating these principles, we further aim to give a broad overview of key results in the field. Many topics have been approached in different ways by different groups; we will not be able to cover all alternative points of view on each topic, but will provide relevant references to original sources and other reviews. Additional key technical details that we expect will be of particular interest for those who wish to begin working in this field can be found in 'The Floquet engineer's handbook'[49], which serves as Supplementary information to this Review. The document will be periodically updated with additional content.

Floquet band structure engineering

We now briefly describe how time-periodic driving can be used to modify the band structure of a quantum particle moving in a spatially periodic lattice potential. The question of how such bands are populated, and a detailed discussion of observables, are addressed in later sections.

The essentials of Floquet theory, including key definitions used below, are summarized in BOX 1. To illustrate the principles of Floquet band engineering we consider a 2D Dirac mode subjected to a uniform, circularly polarized driving field. This model captures the dynamics for crystal momenta in the vicinity of a gapped or gapless Dirac point and provides a building block for describing Floquet engineering in 2D systems such as graphene and transition metal dichalcogenides, as well as 3D TIs. For any given system, the net topological effect of the driving field is determined by its action throughout the entire Brillouin zone, which may include several such Dirac points.

For each value of the momentum $\mathbf{k} = (k_x, k_y)$, the evolution of the system is described by the Bloch Hamiltonian

$$H_{2D}(\mathbf{k}, t) = v[\hbar\mathbf{k} + e\mathbf{A}(t)] \cdot \boldsymbol{\sigma} + \frac{\Delta}{2}\sigma_z, \quad (1)$$

where t is time, v is the velocity of the Dirac electrons, $\mathbf{A}$ is the vector potential, $-e$ is the electron charge, σ_x, σ_y and σ_z are Pauli matrices describing either spin or orbital pseudospin indices, with $\boldsymbol{\sigma} \equiv (\sigma_x, \sigma_y)$, and Δ is the energy gap at $\mathbf{k} = 0$. In the absence of driving, H_{2D} gives rise to dispersion relations $E_c(\mathbf{k})$ and $E_v(\mathbf{k})$ for the conduction and valence bands, respectively, with the pseudo-relativistic form $E_{c,v}(\mathbf{k}) = \pm\sqrt{(\hbar vk)^2 + (\Delta/2)^2}$. In this expression, + and − correspond to the conduction and valence bands, respectively, and $k = |\mathbf{k}|$.

For simplicity we consider a left-hand circularly polarized driving field described by the vector potential $\mathbf{A}(t) = A_0(\cos\omega t, \sin\omega t)$, with driving amplitude A_0 and driving frequency ω. To endow the model with a finite bandwidth, W, we impose a simple cut-off on k such that $|E(k)| < W/2$. In practice, the form of the Hamiltonian and its eigenstates at large values of k, which are important for topological properties, must be found by stitching together multiple Dirac valleys or through a proper termination that respects the periodicity of the Brillouin zone.

For a system with two bands, as described in equation 1, band topology can be visualized geometrically in terms of a unit vector $\hat{\mathbf{n}}(\mathbf{k})$ that relates the band eigenstates $|\psi(\mathbf{k})\rangle$ to points on the Bloch sphere: $\hat{n}_\alpha(\mathbf{k}) = \langle\psi(\mathbf{k})|\sigma_\alpha|\psi(\mathbf{k})\rangle$, where α labels the Cartesian directions x, y and z. In terms of $\hat{\mathbf{n}}(\mathbf{k})$, the integer-valued Chern number $\mathcal{C}$ that characterizes the topology of a given band simply corresponds to the net number of times that $\hat{\mathbf{n}}(\mathbf{k})$ covers the Bloch sphere as $\mathbf{k}$ scans over the entire Brillouin zone, $\mathcal{C} = \frac{1}{4\pi}\oint_{BZ} d^2k\ \hat{\mathbf{n}} \cdot (\partial_{k_x}\hat{\mathbf{n}} \times \partial_{k_y}\hat{\mathbf{n}})$.

Box 1 | **Floquet–Bloch theory basics**

Time evolution in a periodically driven quantum system is governed by the Schrödinger equation

$$i\hbar\frac{\mathrm{d}}{\mathrm{d}t}|\psi(t)\rangle = H(t)|\psi(t)\rangle,\ H(t) = H(t+T), \tag{3}$$

where $|\psi(t)\rangle$ is the state of the system at time t, and the time-dependent Hamiltonian $H(t)$ is periodic in time, with driving period T. The driving frequency is defined as $\omega = 2\pi/T$, although higher harmonics may be involved. According to Floquet's theorem[2], the Schrödinger equation 3 admits a complete set of orthogonal solutions of the form $|\psi(t)\rangle = \mathrm{e}^{-i\varepsilon t/\hbar}|\Phi(t)\rangle$, with $|\Phi(t)\rangle = |\Phi(t+T)\rangle$. Here the quasienergy, ε, plays a role analogous to that of the energy of a Hamiltonian eigenstate in a non-driven system. Owing to the periodicity of $|\Phi(t)\rangle$, it is often useful to express $|\psi(t)\rangle$ in terms of a Fourier series:

$$|\psi(t)\rangle = \mathrm{e}^{-i\varepsilon t/\hbar}\sum_m \mathrm{e}^{-im\omega t}|\phi^{(m)}\rangle. \tag{4}$$

The Fourier sideband components $\{|\phi^{(m)}\rangle\}$ encode the dressing of the system's states by the drive, where the integer m labels the different sideband components. Here, m indicates sideband harmonics and ω is the frequency of the probing field.

The Floquet spectrum (also known as the quasienergy spectrum) is determined by the one-period evolution operator $U(T) = \mathcal{P}\mathrm{e}^{-(i/\hbar)\int_0^T \mathrm{d}t\, H(t)}$, where $\mathcal{P}$ denotes time ordering (also known as path ordering): $U(T)|\psi(0)\rangle = \mathrm{e}^{-i\varepsilon T/\hbar}|\psi(0)\rangle$. For a particle moving in a crystalline lattice potential, the Floquet spectrum is organized into bands, analogous to those of a non-driven system[49,174].

In direct analogy with the emergence of a crystal momentum Brillouin zone for a particle in a periodic potential, all independent solutions of the Schrödinger equation may be indexed by quasienergy values that fall within a single Floquet–Brillouin zone, $\varepsilon_{\min} \le \varepsilon < \varepsilon_{\min} + \hbar\omega$. (Note that $\mathrm{e}^{-i(\varepsilon+n\hbar\omega)T/\hbar} = \mathrm{e}^{-i\varepsilon T/\hbar}$ for any integer n.) In this Review, we take $\varepsilon_{\min} = 0$ or $\varepsilon_{\min} = -\hbar\omega/2$, depending on the context. The unique topological phenomena that occur in Floquet systems, without analogues in equilibrium, owe their existence to the periodicity of quasienergy.

For many cases, it is useful to relate the Floquet operator $U(T)$ to the evolution of a system with a static, effective Hamiltonian, H_{eff}: $U(T) \equiv \mathrm{e}^{-iH_{\mathrm{eff}}T/\hbar}$. The stroboscopic evolution described by $U(T)$ is identical to that described by evolution with H_{eff} for time T. In this Review, we first present two simple cases where the effects of the driving field can be considered perturbatively, allowing the properties of H_{eff} to be heuristically inferred. These cases show that even a weak drive can be used to construct an effective Hamiltonian with topological properties that differ from those of the system in the absence of driving. Beyond the weak-driving regime, Floquet–Bloch systems may show a variety of interesting properties, which are highlighted in this Review.

The integrand in this expression is the band's Berry curvature[50]. The goal of topological Floquet band engineering is to dynamically manipulate the configurations of $\hat{\mathbf{n}}(\mathbf{k})$ in momentum space to induce transitions where, for example, $\hat{\mathbf{n}}(\mathbf{k})$ exhibits a trivial configuration for the non-driven system ($\mathcal{C} = 0$), but is non-trivial for the system's Floquet bands in the presence of the drive ($\mathcal{C} \neq 0$).

We now introduce two key paradigms for inducing topological transitions through, first, off-resonant and, second, resonant driving fields. For gapless systems such as graphene, an off-resonant drive can be used to open a gap and thereby induce non-trivial topology in the system's band structure[8,51]. For a gapped system, such as a band insulator or a semiconductor, a resonant drive may be used to induce a band inversion[10,52]. In both cases, as we now explain, the form of the drive and the properties of the material's original band structure determine the topology of the Floquet bands in the presence of the drive.

We first consider the case of gap opening by an off-resonant drive, using graphene as an example. In graphene, the band structure near zero energy is characterized by two Dirac valleys centred at the K and K′ points at opposite corners of the Brillouin zone. In valley K, the band structure is described by $H_{2\mathrm{D}}$ in equation 1 with $\Delta = 0$; the Hamiltonian near K′ is similar, with $\sigma_y \to -\sigma_y$. If the drive frequency, $\hbar\omega$, is large compared with the single-particle bandwidth, W, such that $\hbar\omega \gg W$, the drive cannot resonantly couple states in the valence and conduction bands for any value of $\mathbf{k}$ in the Brillouin zone (FIG. 1a). In this case, the drive lifts the degeneracies at the Dirac points where the valence and conduction bands touch. At $\mathbf{k} = 0$, relative to the Dirac points in the K (+) and K′ (−) valleys, the Hamiltonian takes the simple form of a pure rotating field: $H^{\pm}_{2\mathrm{D}}(\mathbf{k}=0,t) = A_0\cos(\omega t)\sigma_x \pm A_0\sin(\omega t)\sigma_y$. Although the time average of $H^{\pm}_{2\mathrm{D}}(\mathbf{k}=0,t)$ vanishes, the fact that the Hamiltonian does not commute with itself at different times leads to the emergence of a term proportional to σ_z in the corresponding effective Hamiltonian[51], H_{eff} (see BOX 1 for definition). This term opens up a gap, Δ_{F}, at the Dirac points (FIG. 1a). For further insight into this mechanism of gap opening through an off-resonant drive, see Supplementary information[49].

Importantly, the signs of the σ_z terms induced by the circularly polarized field are opposite in the two valleys. Due to the opposite signs, the induced Berry curvatures add together to yield Floquet bands with non-vanishing Chern numbers[8,51], $\mathcal{C} = \pm 1$. The approximate magnitude of the induced gap can be inferred from second-order perturbation theory: through virtual absorption and emission of a photon from the driving field, a splitting of magnitude $\Delta_{\mathrm{F}} \approx 2(\hbar v e|E_0|)^2/(\hbar\omega)^3$ is induced, where $|E_0| = |A_0|\,/\,\omega$ is the electric field amplitude of the drive[49,51].

For a trivial band insulator or semiconductor, in which the bands are separated by an energy gap Δ, changing band topology requires inducing a band inversion. Such a band inversion can be created in the Floquet spectrum (see BOX 1 for definition) by using a resonant drive with a frequency larger than the bandgap and smaller than the bandwidth[10], W, such that $\Delta < \hbar\omega < W$. In this regime, the drive resonantly couples states on the $\mathbf{k}$-space 'resonance ring', $E_{\mathrm{c}}(\mathbf{k}) - E_{\mathrm{v}}(\mathbf{k}) = \hbar\omega$. The effect of the resonant drive is most easily visualized by transforming to a rotating frame: $|\psi_{\mathrm{R}}(t)\rangle = R(t)|\psi(t)\rangle$, with $R(t) = \mathrm{e}^{-i\omega t P_-}$, where P_- is a projector onto the (unperturbed) negative energy band of $H_{2\mathrm{D}}$ in equation 1 with $\mathbf{A} = 0$. In the rotating frame, the lower band is shifted up in energy by $\hbar\omega$ (FIG. 1b). The driving field (which obtains a d.c. component in the rotating frame) induces a Rabi-like splitting between the two bands, opening a Floquet gap proportional to $|E_0|/\omega$ all the way around the resonance ring. Within the rotating-wave approximation, remaining oscillating terms in the rotating frame are discarded; these residual terms are responsible for multiphoton resonances, which are discussed later. For momenta within the resonance ring defined above, the spectrum obtained from the rotating-wave approximation closely matches that of H_{eff} defined in BOX 1.

Importantly, the characters of the states near $\mathbf{k} = 0$ (which may be either valence-band-like or conduction-band-like) in the reconfigured upper and lower bands described above are swapped compared with those of

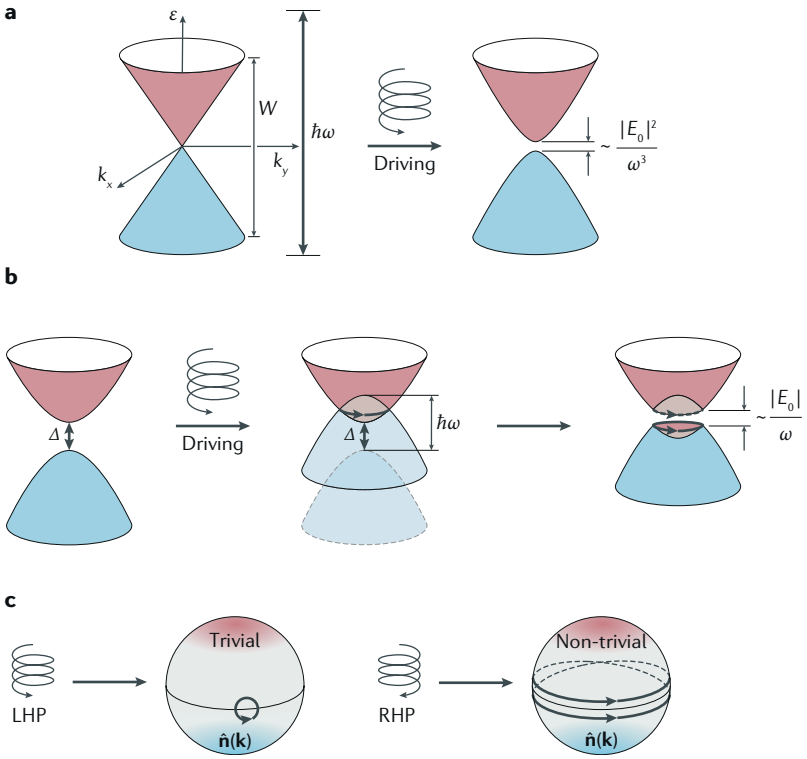

Fig. 1 | **Floquet band engineering for gapless and gapped systems. a** | Off-resonant driving for a gapless system, with $\hbar\omega \gg W$, where $\hbar\omega$ is the driving frequency and W is the bandwidth. The energy dispersion $\mathcal{E}$ is plotted as a function of momentum $\mathbf{k} = (k_x, k_y)$. Circularly polarized light induces a gap in a 2D Dirac dispersion via an off-resonant process involving the absorption and re-emission of a drive photon. The induced gap is proportional to the intensity of the driving electric field, $|E_0|^2$. The induced Berry curvature is concentrated near the band extrema. For graphene, the K and K′ valleys exhibit Berry curvatures with identical signs (determined by the handedness of the drive), leading to Chern numbers of ±1 of the Floquet bands in the absence of resonances. **b** | Resonant driving for a gapped system, with $\Delta < \hbar\omega < W$, where Δ is the energy gap in the absence of the drive. Consider a spin–orbit coupled direct bandgap semiconductor subjected to circularly polarized light. In a rotating frame, the drive opens a gap along the contour of resonant transitions between the valence and conduction bands. The bands obtained in the rotating-wave approximation exhibit a band inversion. **c** | For a two-band system, the Chern number is equal to the winding number of the pseudospin $\hat{\mathbf{n}}(\mathbf{k})$ of the Floquet bands around the polar axis of the Bloch sphere as the momentum $\mathbf{k}$ traverses the resonance contour. When the pseudospin winding of the original bands and the polarization of the driving field (right-hand polarized, RHP, or left-hand polarized, LHP) have the same chirality, $\hat{\mathbf{n}}(\mathbf{k})$ acquires a winding of ±2. When the chiralities are opposite, the winding (and hence Chern number) vanishes.

the non-driven system (FIG. 1b). However, to determine whether a topological band inversion has occurred, it is necessary to check the behaviour of $\hat{\mathbf{n}}(\mathbf{k})$ over the entire Brillouin zone. For a topological transition to occur, the Floquet bandgap must close somewhere in the Brillouin zone as the driving frequency is swept from values $\hbar\omega < \Delta$, where there is no single-photon resonance, to $\hbar\omega > \Delta$, where the characters of the bands near $\mathbf{k} = 0$ are swapped. A gap closing occurs for the Dirac model (equation 1) if the matrix element coupling the two bands in the rotating frame vanishes at $\mathbf{k} = 0$. For a gapped graphene or transition metal dichalcogenide-like system with two valleys as described above, with $\Delta > 0$ and a left-hand circularly polarized drive, a non-vanishing coupling persists at $\mathbf{k} = 0$ in valley K; thus the two bands always repel and the gap never closes. In valley K′, however, the coupling vanishes at $\mathbf{k} = 0$, thus allowing a gap closing and true band inversion to occur[53]. By explicit calculation one can check that in this case the phase of the coupling winds twice (that is, through 4π) as $\mathbf{k}$ goes around the resonance ring; as a result, the Chern numbers of the Floquet bands differ by ±2 from those of the non-driven system[10]. Similar considerations apply for $\Delta < 0$ or for a right-hand polarized drive (FIG. 1c).

Many aspects of Floquet engineering of topological bands have been studied both theoretically and experimentally. Graphene irradiated with mid-infrared circularly polarized light exhibits both the resonant and off-resonant gap-opening mechanisms described above[54–56]. At lower frequencies, multiphoton resonances between the valence and conduction bands affect both the magnitudes of and the numbers of edge states traversing the Floquet gaps at quasienergies $\varepsilon = 0$ and $\varepsilon = \hbar\omega/2$ (REFS[57,58]). Strong drive amplitudes may lead to new topological transitions, which are not captured by the perturbative arguments discussed here[59,60]. Further works have described new driving mechanisms, such as driving through the phonons of honeycomb lattices[61], as well as topological Floquet engineering in 1D[62–64] and 3D[52,65–68]. A variety of approaches for inducing topological states have been explored in photonics[46], acoustics[69] and cold atoms in optical lattices[44,45,70,71].

Topology of Floquet bands

In simple cases, such as in the limit of high-frequency driving, the effective Hamiltonian approach fully captures the topological features of Floquet–Bloch bands. In these cases, the existence of topological edge states at sample boundaries may be inferred by computing the standard non-driven system invariants for the Floquet bands[72,73]. However, there are many important cases where this approach fails. From a conceptual point of view, these cases reveal the possibilities for realizing qualitatively new types of topological phenomena in periodically driven systems.

The main reason why an effective Hamiltonian may fail to capture the topological features of a Floquet–Bloch system is that the spectrum of a Hamiltonian is defined on the entire real line, whereas a Floquet spectrum is defined on a compact (periodic) Floquet–Brillouin zone. Owing to the periodicity of quasienergy in a Floquet system, there is no top or bottom of the spectrum and a continuous band of quasienergies may wind around the Floquet–Brillouin zone an integer number of times as any crystal momentum component traverses the Brillouin zone (FIG. 2a); no such notion of winding exists for energy, which is defined on an open domain.

The physical importance of quasienergy winding is transparently manifested for 1D systems. In 1983, David Thouless showed that the charge pumped through a gapped 1D system subjected to a cyclic, adiabatic modulation of parameters is quantized in units of the fundamental charge, per driving cycle[74]. The quantization is of a topological nature and is insensitive to the details of the driving cycle, provided that the gap remains open (and thereby that adiabaticity is preserved) throughout the cycle.

In the language of Floquet bands, Thouless' quantized adiabatic charge pump described above, often simply referred

to as the Thouless pump, precisely corresponds to the case where the quasienergies exhibit a non-trivial winding as the crystal momentum k runs from $-\pi/a$ to π/a, where a is the lattice constant of the system (FIG. 2b). The quantization of pumped charge follows from the fact that the average group velocity of a Floquet band, $\bar{v}_g$, is proportional to the quasienergy winding number of the band, $\mathcal{W}$:

$$\bar{v}_g = \frac{a}{2\pi\hbar}\oint \mathrm{d}k \frac{\mathrm{d}\varepsilon}{\mathrm{d}k} = a\mathcal{W}/T,$$

where T is the driving period (BOX 1). Thus, for a fully filled band, the average particle displacement over one period, $\overline{\Delta x} = \bar{v}_g T$, is equal to the integer $\mathcal{W}$ times the lattice constant, a. In each cycle, $\mathcal{W}$ units of charge are pumped through the system[9].

The notion of quasienergy winding suggests a natural form for a topological invariant of the Floquet operator

$$U_{1D}(k, T) \equiv \mathcal{P} e^{-(i/\hbar)\int_0^T \mathrm{d}t\, H_{1D}(k,t)},$$

where $\mathcal{P}$ denotes time ordering (also referred to as path ordering) and $H_{1D}(k,t)$ is the time-periodic Bloch Hamiltonian of the 1D system[9]:

$$\nu_1 = \frac{1}{2\pi}\oint \mathrm{d}k\, \mathrm{Tr}[U_{1D}(k,T)^\dagger i\partial_k U_{1D}(k,T)].$$

The invariant ν_1 is a special case of the GNVW index, defined for a generic local unitary time step operator in a 1D system[75]. Physically, ν_1 counts the net winding number of all of the Floquet bands of $U_{1D}(k,T)$; according to the arguments above, it captures the net flow of particles generated by the time evolution of a system in which all fermionic modes are filled. Interestingly, the 3D generalization of this winding number[9] is linked to magneto-electric pumping[76,77].

Although there are local unitary operators for which the GNVW index can take non-zero values, these indices must vanish for any unitary evolution arising from time evolution under a finite, local Hamiltonian

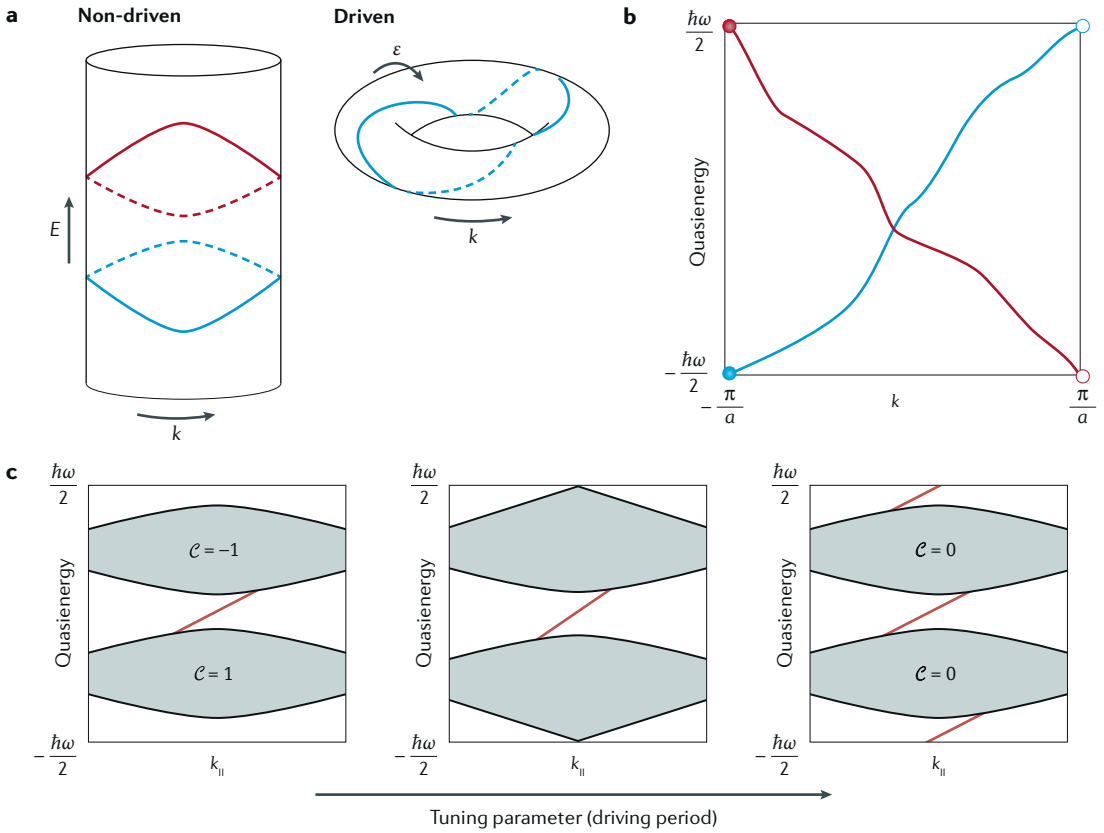

Fig. 2 | **Topological features of Floquet bands without analogues in non-driven systems. a** | In a non-driven system, the energy spectrum $E(k)$ is real-valued. The sketch on the left shows energy, E, as a function of the electronic crystal momentum, k, for a one-dimensional system. As shown on the right, with periodic driving, the quasienergy spectrum $\varepsilon(k)$ is periodic and thus Floquet bands may exhibit a topological quasienergy winding as k traverses the Brillouin zone, $-\pi/a \leq k < \pi/a$. Here, a is the lattice constant of the system. **b** | Floquet band description of Thouless' quantized adiabatic charge pump. Quantized pumping arises from a fully filled chiral Floquet band with non-trivial winding. Such bands with non-trivial winding are obtained in the adiabatic limit, where hybridization between counterpropagating Floquet modes vanishes. **c** | Floquet zone-edge topological transition in a 2D system that in the absence of driving hosts bands with Chern numbers $\mathcal{C} = \pm 1$. When the driving-field photon energy, $\hbar\omega$, is larger than the bandwidth, W, the drive has only a small quantitative effect on the band structure (left). As the driving period is increased, thus lowering $\hbar\omega$, the top and bottom of the spectrum meet at the Floquet zone edge when $\hbar\omega = W$, where W is the bandwidth (middle). When the driving period is increased further, a gap may open at the Floquet zone boundary, resulting in Floquet bands with $\mathcal{C} = 0$ (right). Despite the fact that the Chern numbers of all bands vanish, topologically protected anomalous chiral edge states propagate along system boundaries.

(in strictly 1D), see Supplementary information[49]. For the Thouless pump, this implies that the quasienergy spectrum must host bands with winding numbers of opposite sign, which necessarily cross (FIG. 2b). Generically, these crossings are avoided owing to hybridization, yielding bands with trivial winding ($\mathcal{W}=0$). However, these hybridization gaps close exponentially in $1/\omega$ as $\omega \to 0$, allowing chiral bands (with $\mathcal{W}\neq 0$) to emerge in the adiabatic limit.

In addition to opening the possibility for quasienergy winding of individual Floquet bands, the periodicity of quasienergy also provides new channels through which topological transitions can occur. In a non-driven system, a topological transition occurs through the closing and reopening of the bandgap as a parameter (such as quantum well width[78]) is tuned through a critical value. In a driven system, there is an additional gap at the Floquet–Brillouin zone edge ($\varepsilon = \pm\hbar\omega/2$), which allows the closing and reopening of a degeneracy between the bottom of the lowest Floquet band and the top of the highest band, for a given choice of Floquet zone. Through the closing and reopening of the quasienergy gap at the Floquet–Brillouin zone edge, novel topological phases without analogues in equilibrium systems can be realized in periodically driven systems. The topological properties of such systems cannot be captured by the topological invariants (such as Chern numbers) that characterize equilibrium, non-driven systems; they are therefore referred to as anomalous Floquet phases.

A topological transition leading to an anomalous Floquet phase is illustrated in FIG. 2c. In the absence of driving, the system hosts topologically non-trivial bands with Chern numbers ±1 (left panel). With driving, the Chern numbers of both of the resulting Floquet bands become trivial, $\mathcal{C}=0$ (right panel). Crucially, despite finding trivial topological indices for the Floquet bands of $U(T)$, the system remains topologically non-trivial. To see this, consider the fate of the topological edge states that existed in the gap of the system before the driving was introduced. Throughout the sequence of driving frequencies considered in FIG. 2c, the original gap (between the bottom of the conduction band and the top of the valence band) never closes; therefore, the transition to the configuration with $\mathcal{C}=0$ cannot cause the original edge states to disappear. From general arguments about spectral flow, the net chiralities of edge states above and below a given band must be equal to the Chern number of the band[79,80]. Thus, we conclude that the system must host chiral edge states in both of its gaps, near $\varepsilon=0$ and $\varepsilon=\pm\hbar\omega/2$, despite having trivial Chern indices. In such cases, the non-trivial topology of the Floquet system is encoded not in the bulk Floquet spectrum itself, but rather in the micromotion that occurs within the driving period[24–27,81]. Topological edge states that appear in systems with trivial Floquet operators are referred to as anomalous edge states.

As the example above shows, the Chern numbers of Floquet bands do not provide sufficient topological information to predict the absolute numbers of chiral edge states that appear within each gap. This is true both for anomalous phases with vanishing Chern numbers, described above, and for systems with non-vanishing Chern numbers. In particular, this subtlety arises when single-photon or multiphoton resonances are involved. The extension of the topological characterization of Floquet systems to include symmetries is discussed in BOX 2.

Experimentally, the unique aspects of topology in Floquet systems, which do not have analogues in non-driven, equilibrium systems, have been investigated for optical, cold atomic and solid-state systems. In the optical domain, 1D discrete-time quantum walks with chiral symmetry provided the first demonstration of anomalous '0' and 'π' edge states[82]. Waveguide arrays with periodic modulations along the propagation axis[83], and microwave resonator arrays[84] have also been used to demonstrate the emergence of anomalous topological Floquet edge modes in 1D[85] and 2D[84,86,87]. In cold atoms, 1D Thouless pumps realizing non-trivial quasienergy winding were recently realized in fermionic[88] and bosonic[89] systems. Realizations of 2D anomalous phases (FIG. 2c) have been proposed for cold atoms[90,91]. One-dimensional systems with '0' and 'π/T' Majorana modes have also been proposed to be realized for systems of cold atoms[62] and Josephson junctions[92].

Many-body dynamics in Floquet systems

The discussion so far has focused on single-particle Floquet–Bloch bands in the presence of a drive. Whether the Floquet bands provide a useful starting point for describing the dynamics of the system depends on the extent to which the physical properties of the system are simply described within this basis. The remainder of this Review is devoted to characterizing the physical properties and observables of periodically driven many-body systems, and the conditions under which driving allows new topological phenomena to be observed via transport or spectral measurements.

Mesoscopic transport in Floquet systems. We now discuss signatures of drive-induced topological Floquet edge states in mesoscopic transport. The mesoscopic setup consists of a driven electronic system that is connected to two or more leads. The driving field acts only on the system and does not directly affect the leads. The electrons within each lead, λ, are assumed to be described by a Fermi–Dirac distribution with a well-defined chemical potential and temperature. We focus on the regime where the transit time for an electron through the system is short compared with the timescales associated with electron–electron scattering and inelastic scattering due to coupling to phonons or other environmental degrees of freedom. Under these conditions, the electronic state within the system is fully controlled by the distributions in the reservoirs, and the system's two-terminal or multi-terminal conductance is given by the Floquet–Landauer formula.

The Floquet–Landauer approach has been used to study transport through a variety of topological driven systems[51,54,57,93–98]. For a non-driven system, the Landauer formula relates current to the Fermi distributions of the leads and to the energy-dependent transmission probability (for the case of two-terminal transport), $\mathcal{T}(\mathcal{E})$, where $\mathcal{E}$ is the energy of the incoming

(or outgoing) states. In a driven system, electrons may coherently absorb or emit energy in multiples of the driving field quantum $\hbar\omega$ as they pass through the system. As a result, the transmission probabilities $\mathcal{T}^{(j)}_{\mathrm{RL}}(\mathcal{E})$ and $\mathcal{T}^{(j)}_{\mathrm{LR}}(\mathcal{E})$ between the left (L) and right (R) leads depend on the incident energy $\mathcal{E}$ and an additional integer-valued index, j, that counts the net number of photons absorbed during the electron's transit through the system. The difference between energies of the incoming and outgoing states is equal to $j\hbar\omega$. In terms of the Floquet transmission probabilities, the two-terminal current (from the left lead to the right lead) is given by:

$$I = \frac{-e}{h}\int_{-\infty}^{\infty} \mathrm{d}\mathcal{E} \sum_j \{\mathcal{T}^{(j)}_{\mathrm{RL}}(\mathcal{E}) f_{\mathrm{L}}(\mathcal{E}) - \mathcal{T}^{(j)}_{\mathrm{LR}}(\mathcal{E}) f_{\mathrm{R}}(\mathcal{E})\}, \quad (2)$$

where $f_{\mathrm{L}}(\mathcal{E})$ and $f_{\mathrm{R}}(\mathcal{E})$ are the Fermi–Dirac distributions in the left and right leads, respectively, and h is Planck's constant.

The transmission probabilities $\mathcal{T}^{(j)}_{\mathrm{RL}}(\mathcal{E})$ and $\mathcal{T}^{(j)}_{\mathrm{LR}}(\mathcal{E})$ can be expressed in terms of the Floquet Green's function of the open, driven system (including the effects of its coupling to the leads)[99]. Through this connection, transport through the driven system can be related to its quasienergy spectrum; in particular, this formalism and its generalization for multi-terminal transport provide the basis for describing the transport signatures of Floquet gap opening and the appearance of topological Floquet edge modes[51,54,57,93–97].

The two-terminal transport signatures of drive-induced topological gap opening in graphene[8,51] are more subtle than one may anticipate based on analogies to equilibrium topological materials[57]. In the case of a low-frequency driving field, with $\hbar\omega$ much less than the bandwidth, the graphene band structure must be folded down several times to fit within a single quasienergy Brillouin zone. Therefore, in addition to the Floquet gap opened at the original Dirac point of the non-driven system, a hierarchy of increasingly small gaps and associated edge states, resulting from even-order multiphoton resonances, appear near zero quasienergy[57,100]. Transport through the edge states appearing at zero quasienergy yields a non-zero conductance in the large-system size limit. However, in contrast to equilibrium quantum Hall systems, this conductance is not quantized[57].

The reason why chiral Floquet edge modes may not give rise to quantized transport is related to the way that the Floquet edge states couple to the electronic states of the leads[94,96]. In particular, the spectral weight of a Floquet state with quasienergy ε is spread across many sideband components $|\phi^{(m)}\rangle$ (see equation 4 in BOX 1), with energies $\varepsilon + m\hbar\omega$. This spread of energies leads to a complicated relationship between the chemical potentials of the source and drain leads and the populations of the Floquet edge states. The resulting populations do not respect the conditions that yield quantized transport in equilibrium quantum Hall systems.

The time-averaged spectral function[54,101] (see Supplementary information[49] for definition and detailed discussion) provides a helpful way of visualizing the spectral weights of the Floquet states and how they couple to incoming and outgoing states at specific energies in the non-driven leads. We illustrate the time-averaged spectral function for graphene under circularly polarized light in FIG. 3a. The Floquet edge states in the gap opened at the Dirac points are built primarily from states near zero energy and can efficiently couple to states in the lead near $\mathcal{E} = 0$. However, some of the spectral weight of these Floquet edge states is shifted to sidebands near energies $n\hbar\omega$, for integer $n \neq 0$ (FIG. 3b). The spectral weights of these sidebands are controlled by the ratio of the drive amplitude to the photon energy.

Sidebands corresponding to $n \neq 0$ primarily couple to states of the leads whose energies are far from the chemical potential (set near $\mathcal{E} = 0$ to probe transport through the drive-induced topological edge states). Therefore, a small increase (or decrease) of the lead chemical potential around $\mathcal{E} = 0$ does not simply populate (or empty) the states of the edge mode over the corresponding range of quasienergies. As a result, the current flowing in the edge mode due to a voltage bias between the leads is different from what it would be in equilibrium, where the chemical potential of the lead is directly mapped onto the edge state; the corresponding differential conductance deviates from the quantized value of $2e^2/h$ per mode[57], where e denotes the electronic charge. Similar considerations apply to edge states in the driving-induced gap appearing at the Floquet zone edge, $\varepsilon = \pm\hbar\omega/2$, and to higher-order edge states that form in mini-gaps in the quasienergy spectrum due to multiphoton resonances. Such states carry substantial spectral weight at energies far from the chemical potentials of the leads and therefore give non-universal contributions to the differential conductance. Thus, in general, there is no simple relation between differential conductance at a given value of lead

Box 2 | **Symmetries and topology in Floquet systems**

As in non-driven systems, the time-reversal, particle–hole and chiral symmetries[175] that distinguish topological classes can also be implemented in Floquet systems[9,25,26,29,38,81,99,176–180]. A natural way to ensure that the Floquet operator $U(T)$ obeys one or more of these symmetries is to impose certain conditions on the evolution operator over all intermediate times $0 \leq t < T$, where t is time and T is the driving period. For example, particle–hole symmetry can be ensured by requiring that the instantaneous Hamiltonian (and hence the evolution operator $U(t)$ for all $0 \leq t < T$) itself possesses particle–hole symmetry[25,62]. This condition is automatically satisfied for the mean-field (Bogoliubov–de Gennes)[181] evolution describing any superconducting system. Time-reversal and chiral symmetries can be implemented by enforcing time non-local symmetries on the evolution[25,81,99,176]: $U(t) = SU(t_* - t)U^{\dagger}(t_*)S^{-1}$, where t_* denotes a special point in the driving cycle, and chiral (time-reversal) symmetry is ensured by taking S to be a unitary (antiunitary) operator. With the Altland–Zirnbauer symmetry classes implemented in this way for the driven case, the same classes allow for topologically non-trivial bands with and without driving[25,26]. Importantly, however, driven systems support a richer set of possibilities within each non-trivial symmetry class, owing to the possibility of different micromotion phases that may host anomalous edge states[24–26,81] (see main text). Moreover, new types of non-symmorphic spacetime symmetries (combining time translations with spatial symmetry operations) may also protect topological features of Floquet–Bloch bands[182–184].

Prominent examples of anomalous Floquet phases in the presence of symmetries have been discussed for 1D systems[62,82,177,185,186]. These systems host new types of topological bound states at sample edges, with protected quasienergy values of 0 and/or $\hbar\omega/2$. When both 0 and π modes are present simultaneously, the spectrum exhibits a protected quasienergy splitting of $\hbar\omega/2$ that gives rise to robust oscillations with precisely twice the driving period (see main text for the connection to Floquet time crystals). In the superconducting case, these π-Majorana modes may yield new routes to braiding non-Abelian particles in a strictly 1D system[187].

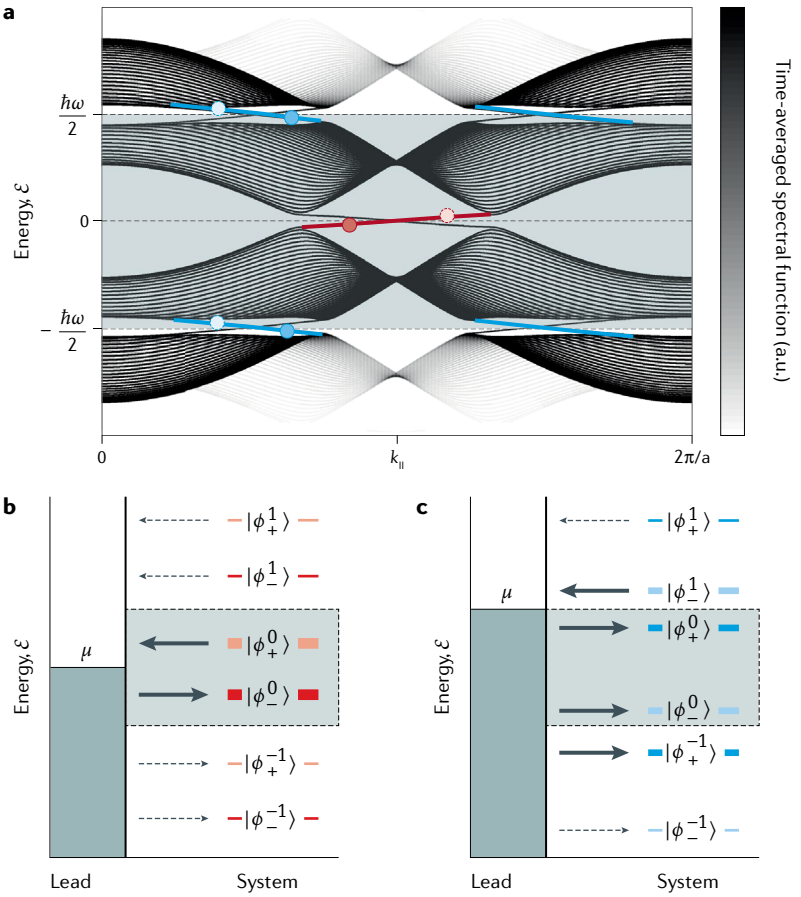

Fig. 3 | **Edge state transport in Floquet topological insulators. a** | Time-averaged spectral function of a graphene strip driven by circularly polarized light, as a function of the crystal momentum component $k_{\parallel}$ parallel to the strip. The blue-shaded region marks the Floquet–Brillouin zone. The time-averaged spectral function helps to visualize the frequency content of the Floquet states, which governs their coupling to external leads. Here, a is the lattice constant of graphene. **b** | Tunnelling between a Fermi reservoir and edge states $|\psi_-\rangle$ and $|\psi_+\rangle$ at two values of $k_{\parallel}$ in the gap around energy $\mathcal{E} = 0$ (dark and light red dots in part **a**). The dominant Fourier components of $|\psi_-\rangle$ and $|\psi_+\rangle$ are centred near the chemical potential, μ, which is set to $\mathcal{E} = 0$. The filled and empty states of the lead near $\mathcal{E} = 0$ predominantly fill (empty) the Floquet states $|\psi_-\rangle$ and $|\psi_+\rangle$ at negative (positive) quasienergies. However, the harmonic components $|\phi_-^{(\pm1)}\rangle$ and $|\phi_+^{(\pm1)}\rangle$ near $\mathcal{E} \approx \pm\hbar\omega$ (see equation 4) open channels for electrons to tunnel into (out of) the nominally empty (filled) states, as indicated by the small dotted arrows. These additional photon-assisted tunnelling processes spoil the ideal filling of the Floquet edge modes and the perfect quantization of edge transport. **c** | Edge states in the gap around $\mathcal{E} = \pm\hbar\omega/2$ (dark and light blue dots in part **a**) are composed of roughly equal superpositions of the valence and conduction bands of the non-driven system. When the chemical potential of the lead is centred in the gap at $\mathcal{E} = \hbar\omega/2$, all states in the edge mode experience substantial coupling to filled states of the lead owing to their large valence-band components. As a result, these chiral Floquet edge modes do not mediate precisely quantized transport[94,96].

chemical potential and the number of chiral edge states in a corresponding quasienergy gap[94,96].

In some cases, new types of quantized transport phenomena beyond zero-bias conductance have been found for driven systems. For example, the appearance of Floquet–Majorana edge modes[62] at the end of a periodically driven 1D superconductor does not give rise to a quantized differential conductance at zero bias, as it does in the equilibrium case[102,103]. Rather, for a system with a Floquet–Majorana mode at quasienergy $\varepsilon = 0$ or a Floquet π-Majorana mode at $\varepsilon = \hbar\omega/2$, the differential conductance $\sigma(\mu)$ summed over the discrete set of lead chemical potentials (or back gate potentials) $\mu_n = \varepsilon + n\hbar\omega$, for all integers n, yields the quantized value[93] $2e^2/h$. Perfect quantization of the conductance mediated by the Floquet edge states of a 2D FTI is also recovered through an analogous sum rule[96,98].

As discussed above, the presence of chiral Floquet edge modes around the perimeter of a 2D system does not guarantee a quantized Hall conductance at low bias. However, the anomalous 2D phase depicted in FIG. 2c offers a new possibility of quantized current at large source–drain bias. Specifically, in the presence of disorder, the anomalous 2D system's Floquet bands (all with Chern number zero) become fully localized, while the system's chiral edge modes persist[104]. In a non-driven system, delocalized states are needed to provide a spectral termination for chiral edge modes. In a Floquet system, however, a chiral edge state can wind around the quasienergy Brillouin zone and terminate on itself, analogous to the 1D winding bands in FIG. 2a,b. At large source–drain bias, one of the chiral Floquet modes of this anomalous Floquet–Anderson insulator (AFAI) may become completely filled, whereas the mode propagating in the opposite direction is completely empty. In this situation, the system hosts a quantized current[97,104], for analogous reasons to those described for the Thouless pump. In contrast to the situation of a truly 1D system (FIG. 2b), the counterpropagating chiral edge modes of a 2D AFAI are spatially separated and therefore exhibit exponentially small quasienergy splittings in the sample width, even at finite driving frequency. This property allows the 2D AFAI, with a fully localized bulk, to carry a quantized current, even in the non-adiabatic driving regime[97,104]. Beyond transport current, signatures of light-induced chiral edge states may also appear in magnetization measurements[105,106]. For the 2D AFAI, the magnetization density is quantized, providing means to measure the topological invariant that characterizes the phase using a bulk probe[106].

Transient dynamics and prethermalization. Early experiments on FTIs in solid-state systems have focused on short-time dynamics through pump–probe measurements[47,48,107]. By focusing on short times, the formation of Floquet–Bloch states can be probed separately from the question of the system's fate at long times. The opening of a topological Floquet gap on the surface of a 3D TI was demonstrated in Bi_2Se_3 using time-resolved angular-resolved photoemission spectroscopy[47]. The temporal emergence of Floquet bands in such pump–probe settings, as manifested in the time-resolved angular-resolved photoemission spectroscopy signal, has also been studied theoretically[60,108–110]. These theoretical works provide helpful insight for interpreting experimental data and illuminate the role of electron–electron interactions in the gap-opening process. More recently, the photoinduced Hall effect has been observed in graphene subjected to circularly polarized light[8,51] using a newly developed high-speed time-resolved transport setup[48]. In cold atom systems, transient dynamics have been used to directly probe band topology through anomalous transport[111,112], quench dynamics[113–115] and heating rates[116].

Although closed, interacting Floquet systems generically heat towards featureless high-entropy density states at long times, the question of when this heating sets in is of crucial importance. Under appropriate conditions to be discussed below, the timescale over which runaway heating occurs may become extremely long[34,117–122]. In such cases, on short to intermediate timescales, the system may attain a (nearly) time-periodic quasisteady state that hosts topological phenomena arising from the underlying Floquet band structure.

One important regime where heating rates can be suppressed is the limit where the drive frequency is large compared with the relevant energy scales in the system (FIG. 4a). In this regime, the driving-field photon energy is much larger than the energy change in any single scattering event in the system. Energy absorption from the drive requires high-order processes involving many-particle rearrangements, known as many-body resonances[123], and is therefore heavily suppressed.

In an idealized setting in which the system has a finite single-particle bandwidth, such as in a lattice with a finite number of orbitals per unit cell, the heating rate may become exponentially suppressed as a function of the drive frequency[124]. However, in any real physical system, the kinetic energy is not bounded from above and higher bands will inevitably be present. The idealized high-frequency limit is therefore never truly realized: the photon energy $\hbar\omega$ (or its integer multiples) necessarily directly connects low-lying bands of interest with higher-energy states. The lifetime of the quasisteady state is therefore also limited by interband transitions — when particles are excited across the gap — to these high-energy states. At high driving frequencies, the rates of these interband transitions are expected to be at least suppressed as a power law[125,126] in $1/\omega$, ensuring that a useful high-frequency regime does exist. This regime is commonly exploited in experiments on cold atoms in optical lattices.

When the high-lying bands are separated from a set of low-lying bands by a large single-particle energy gap Δ, the rates of interband transition (with particles excited across the gap) may be exponentially suppressed for low driving frequencies, $\hbar\omega/\Delta \ll 1$. (Note that this low-frequency driving regime does not imply adiabaticity, since even in the presence of a large gap in the single-particle spectrum the system need not have a many-body gap.) In this regime, many photons must be absorbed (or many particles rearranged within the low-energy sector) for one excitation in the high-energy subspace to be created (FIG. 4b). The minimal order in perturbation theory at which a real transition can occur is thus determined by the ratio of the energy gap, Δ, to the energy change associated with a single scattering event. This latter scale is governed by the local interaction energy scale, U, the single-particle bandwidth of the low-lying bands, W, and the driving-field photon energy, $\hbar\omega$. Thus, we may expect an exponential suppression of the rate of excitations across the gap Δ to the high-energy subspace, with a power controlled by the ratio[121] $\Delta/\max\{W, \hbar\omega, U\}$.

During a time window in which scattering processes involving energy absorption from the drive are absent, one may find a rotating frame in which the system evolves according to a static Hamiltonian[34,117–120,127]. This Hamiltonian is often referred to as the prethermal Hamiltonian, and we denote it here by H_*. In this rotating frame, an ergodic system may thus prethermalize to an equilibrium-like state with respect to H_*. Crucially, the prethermal effective Hamiltonian is not simply the time-averaged system Hamiltonian: H_* may exhibit important qualitative differences from the Hamiltonian of the non-driven system (such as the appearance of a term that opens a gap in graphene). Precisely determining the prethermal effective Hamiltonian for specific systems is a complex theoretical challenge[120,128–130].

Ensuring a long lifetime for the quasisteady state is important for the realization of FTIs in the presence of interactions, in particular for realizing strongly correlated topological phases of matter in Floquet systems. A number of proposals have been made in this direction, including the realization of a fractional Chern insulator[131] phase in strongly driven graphene-like systems[19], as well as interesting magnetic phases in optically driven Mott insulators[132,133]. In such settings, the ramp-up of the drive should furthermore be optimized to achieve prethermal states with suitably low energy density[23].

A qualitatively different quasisteady regime occurs for $\hbar\omega \leq W, U$ and $W, U \ll \Delta$. The conditions $\hbar\omega, W, U \ll \Delta$ ensure that interband transitions are suppressed. However, the system may still rapidly absorb energy and heat up within the low and high energy sectors. After an initial relaxation time, the system reaches a restricted infinite-temperature-like quasisteady state, which is characterized by the maximal local entropy density

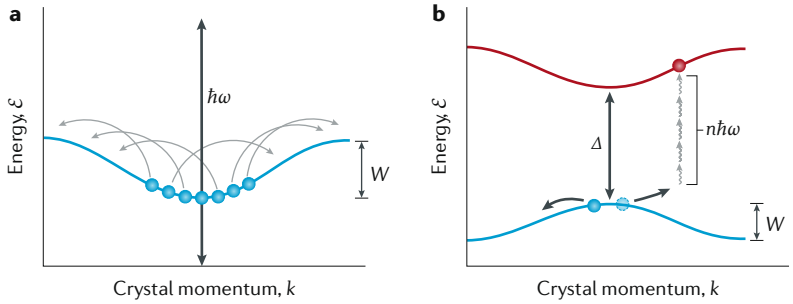

Fig. 4 | **Heating via energy absorption from the drive. a** | When the drive frequency, ω, is large compared with the single-particle bandwidth, W, and the energy scale of local interactions, U, absorption of one driving-field photon of energy $\hbar\omega$ requires a high-order rearrangement of particles in the system. For weak interactions, $U \ll W$, the order of the process is controlled by the ratio $\hbar\omega/W$, which appears as a power in the corresponding transition rate. Therefore, the absorption rate is exponentially suppressed in ω for $\hbar\omega \gg W, U$. **b** | Energy absorption in a system composed of low-energy and high-energy bands, separated by a gap Δ that is much larger than the bandwidth of the low-lying bands, W. For $W, \hbar\omega, U \ll \Delta$, transitions across the single-particle gap Δ can only be excited through processes involving high-order multiphoton absorption and/or rearrangements within the system. The minimal order of the excitation process, n, is governed by the ratio Δ / max $\{\hbar\omega, W, U\}$; for $W, U \leq \hbar\omega$ this implies that the rate for exciting the high-energy degrees of freedom is exponentially suppressed in $1/\omega$. A combination of effects explained in parts **a** and **b** may be utilized in systems with a clear separation of scales, $W, U \ll \Delta$. For such a system, the lifetime of the prethermal state can thus be optimized by working in the regime $W, U \ll \hbar\omega \ll \Delta$, where both the high- and low-frequency conditions are simultaneously satisfied. For cold atoms, such a situation may be arranged, for example, by working with a very deep optical lattice. Heating rates for cold atoms in Floquet–Bloch bands of optical lattices have recently been experimentally characterized[22,111,112,126,173].

subject to the constraint of fixed particle number in each sector. Remarkably, such states may display robust, topological behaviour resulting from the uniform occupation of modes in each Floquet band, which follows from entropy-density maximization. Non-universal features of the system's Floquet spectrum are washed out as observables are averaged over the high-entropy distribution, leaving the global, topological properties on display. For example, in a 1D system with winding quasienergy bands (as in FIG. 2b), the uniform occupation distribution implies that each Floquet band carries a universal current $I = \rho\mathcal{W}/T$, where ρ and $\mathcal{W}$ are the particle density and quasienergy winding number of the band, and T is the driving period;[121] this value of the current is insensitive to all features of the dispersion, other than the winding number, $\mathcal{W}$.

Floquet many-body localization. In well-isolated systems such as cold atoms, the phenomenon of many-body localization (MBL)[134–140] in strongly disordered systems may completely eliminate the system's tendency to absorb energy from the drive, allowing non-trivial stationary states to persist even in the long-time limit. From a conceptual point of view, the possibility of stabilizing long-time steady states of closed, periodically driven, many-body systems enables the sharp delineation of intrinsic phases in Floquet systems[32]. Importantly, MBL is compatible with a variety of symmetry-breaking and topological orders[39–43,137]. Interestingly, FTIs that exhibit protected edge states at quasienergy $\hbar\omega/2$ are closely connected to Floquet MBL phases, known as Floquet time crystals, that break the discrete time-translation symmetry of the system down to an integer multiple of the driving period[32–34,141–145].

For FTIs in two dimensions and above, the necessity of being compatible with MBL severely restricts the possibilities for finding stable intrinsic FTI phases in closed systems. In equilibrium, systems with non-trivial topological indices (such as Chern numbers) necessarily host delocalized states at certain energies. These delocalized states are fundamentally connected with the chiral or helical modes that appear at system boundaries, and cannot be destroyed by disorder without inducing a topological transition into a trivial phase. The presence of delocalized states, even at high energy, generically destabilizes MBL at all energy densities[146]. This leads to the conclusion that FTIs in 2D and 3D, whose Floquet bands carry non-trivial topological indices, are intrinsically unstable in the absence of a bath. However, this argument does not rule out the stability of anomalous Floquet phases[39–42,147,148]. These phases feature topologically protected edge modes coexisting with trivial Floquet bands, and therefore need not host delocalized bulk states[104]. Importantly, the non-trivial, intraperiod micromotion that characterizes these phases is consistent with MBL[149].

Steady states in open Floquet systems. When a driven many-body system is coupled to an environment or external bath(s), it will tend to a steady state where energy and entropy production (heating) due to the drive are balanced by an outflow of these quantities to external baths. This scenario is particularly relevant in the solid state, where electrons are inevitably coupled to environmental degrees of freedom including electromagnetic radiation, phononic modes of the host crystal and possibly external leads that act as particle reservoirs.

In equilibrium, the steady state of an open system takes the universal form of a Gibbs state, fully determined by the temperature and chemical potential of the bath to which it is coupled. Under special conditions, a Floquet system may attain an analogous Floquet–Gibbs steady state, defined by the density matrix $\rho_{\mathrm{FG}} = \mathrm{e}^{-\beta H_{\mathrm{eff}}}/\mathrm{Tr}[\mathrm{e}^{-\beta H_{\mathrm{eff}}}]$, where H_{eff} is defined in BOX 1, and $1/\beta$ is the temperature of the bath[150–152]. Generically, however, such a universal statement cannot be made. Rather, the steady states of Floquet systems are typically sensitive to details of the bath as well as the form of the system–bath coupling. While this added complexity makes non-equilibrium systems challenging to study theoretically, it also opens opportunities for controlling steady states through reservoir engineering (see below).

Physically, for the induced geometric or topological features of a system's Floquet bands to be reflected in its linear response to applied probe fields, the steady state, ρ_{steady}, should take a simple form in terms of populations of the single-particle Floquet states. Suppose for example that a weak probing electric field $\delta\mathbf{E}(\Omega)$ is applied to the system with probe frequency Ω. For $\Omega \ll \omega$, the Floquet–Kubo formula[8,49,153] can be used to obtain the effective a.c. conductivity $\bar{\sigma}_{\alpha\beta}(\Omega)$ appearing in Ohm's law, $\delta J_\alpha(\Omega) = \bar{\sigma}_{\alpha\beta}(\Omega)\delta E_\beta(\Omega)$, where $\delta\mathbf{J}(\Omega)$ is the change in the current density at frequency Ω due to the probe[49]:

$$\bar{\sigma}_{\alpha\beta}(\Omega) = \frac{-1}{\Omega T}\int_0^\infty \mathrm{d}\tau\ \mathrm{e}^{i\Omega\tau} \int_0^T \mathrm{d}t'\mathrm{Tr}\{\rho_{\mathrm{steady}}(t')[J_\alpha(t'+\tau), J_\beta(t')]\} + \frac{1}{i\Omega}\mathcal{K}^{(0)}_{\alpha\beta}(\Omega),$$

where α and β index the Cartesian directions x, y and z, $\rho_{\mathrm{steady}}(t')$ is the time-periodic steady-state density matrix of the system at time t' and $\mathcal{K}^{(0)}_{\alpha\beta}$ is the time-averaged diamagnetic contribution (for a full derivation see Supplementary information[49]).

The expression for the conductivity above reduces to a particularly simple form in the special case where ρ_{steady} obeys Wick's theorem[154] and the corresponding single-particle density matrix is diagonal in the Floquet basis. Here we refer to steady states obeying these conditions as diagonal, but note that generic Floquet systems do not obey such strict conditions[155–157]. For diagonal steady states, the expression for $\bar{\sigma}_{\alpha\beta}$ takes an analogous form to that obtained for weakly interacting electrons in equilibrium, with energies replaced by quasienergies, and the equilibrium Fermi–Dirac distribution replaced by the non-equilibrium populations of the Floquet states[49]. In particular, when the steady state takes on a band-insulator-like form in terms of Floquet band populations, then, as in equilibrium, the Floquet–Kubo formula implies that the bulk Hall conductivity $\bar{\sigma}_{xy}$ is quantized while $\bar{\sigma}_{xx}$ vanishes[8,158]. Transport in Floquet systems can also be treated within a Floquet–Boltzmann approach[159,160], giving similar conclusions.

Given this complicated situation, under what conditions may we hope to stabilize TI-like behaviour in a Floquet system? For illustration, here we consider a resonantly driven 2D single-valley direct bandgap semiconductor, with dispersion at low energies described by the 2D Dirac model of equation 1. Similar reasoning may be applied to gapless (graphene-like) systems, when the drive resonantly couples states away from the Dirac points.

As discussed above, one of the key aims in Floquet band engineering is to use above-bandgap radiation to drive a topological transition by inducing an effective band inversion in the Floquet spectrum (FIG. 1b). In that discussion, we used the rotating-wave approximation to describe the band inversion caused by the first-order resonance between the valence and conduction bands, $E_c(\mathbf{k}) - E_v(\mathbf{k}) = \hbar\omega$. However, for generic drive frequencies, higher-order resonances $E_c(\mathbf{k}) - E_v(\mathbf{k}) = n\hbar\omega$ with $n > 1$ may occur in the Brillouin zone, leading to multiple foldings of the Floquet bands into the quasienergy Brillouin zone. Although the lower Floquet band exhibits the desired structure in the vicinity of the first resonance, at larger momenta, such as in the vicinity of the two-photon resonance and beyond, it contains states arising from high up in the original conduction band (FIG. 5a, right panel). The Floquet–Gibbs insulator state would then host a finite density of electrons and holes at very high energies. This situation is highly unstable, and therefore the Floquet–Gibbs insulator state cannot be obtained under realistic physical conditions. As we show below, a steady state obtained under realistic conditions can nonetheless exhibit TI-like behaviour.

From a physical point of view, in the regime in which the drive amplitude is small compared with $\hbar\omega$, one may expect states deep in the valence band to remain occupied in the presence of the drive (with only weak modifications due to off-resonant hybridization with the conduction band). In this case, the steady state is expected to take the form of the generalized Floquet insulator state depicted schematically in the right panel of FIG. 5a. For small momenta up to the vicinity of the second (two-photon) resonance, the populations correspond to a filled Floquet band, whereas at larger momenta, the electronic populations follow perturbatively modified valence-band-like states, rather than the folded Floquet bands.

In the generalized Floquet insulator state, the single-particle density matrix for momenta within and in the vicinity of the single-photon resonance ring, $E_c(\mathbf{k}) - E_v(\mathbf{k}) = \hbar\omega$, is diagonal in the Floquet basis and features populations only in the lower Floquet band. In particular, the form of the single-particle density matrix is maintained at the resonance ring itself, where the original valence and conduction bands are strongly hybridized. This property is essential for observing topological phenomena in FTIs, as the drive-induced Berry curvature is strongly localized in the vicinity of the resonance ring. Achieving this condition requires a driving amplitude large enough that the induced Floquet gap exceeds the scattering rates in the steady state; this condition ensures that the separation between Floquet bands exceeds the quasiparticle lifetime broadening in the steady state. Owing to the drive-induced band inversion, the generalized Floquet insulator state hosts a population inversion with respect to the original bands for momenta within the resonance ring. Experimentally, substantial population inversions (referred to in the literature as electron–hole plasmas) can be maintained even for a weak drive for which the Floquet gap cannot be resolved[161–163], and have been exploited in semiconductor lasers[164–166].

We now discuss the conditions under which a generalized Floquet insulator state can be approximately maintained. These conditions are revealed by examining the population kinetics of electrons in an FTI connected to (zero temperature) heat baths consisting of acoustic phonons and the electromagnetic environment[167–169] (FIG. 5b). Higher-order resonances are expected to play a minor role for relatively weak driving. Therefore, for simplicity, we consider a parameter regime where only a single resonance is supported in the system[168] (FIG. 5a, left panel). In this situation, the generalized Floquet insulator state and the Floquet–Gibbs insulator state coincide. The details of the distribution near higher-order resonances and the corresponding implications for the system's response remain important directions for investigation.

As emphasized in the sections above, a crucial aspect of Floquet systems is that the quasienergy is defined only modulo multiples of the driving-field photon energy, $\hbar\omega$. Beyond the usual kinematic constraints on scattering processes of non-driven systems, the periodicity of quasienergy allows for scattering processes (known as Floquet–Umklapp scattering processes) in which the total initial quasienergy of the particles and bath modes differs from the total quasienergy of the outgoing particles and bath modes by an integer multiple of $\hbar\omega$. In particular, these quantum Floquet heating processes[170] spontaneously scatter electrons from the lower to the upper Floquet band at zero bath temperature, a process that would be impossible in the bands of a non-driven system in thermal equilibrium. The impact of these processes on the steady state of the system is therefore substantial, leading to important deviations from the ideal Floquet insulator distribution described above.

Note that by shifting the choice of Floquet–Brillouin zone (by changing the value of ε_{min}, see BOX 1), the ordering of bands can be interchanged; the definition of what is called a Floquet–Umklapp process thus also depends on the choice of Floquet–Brillouin zone. This is only a matter of terminology: as long as all physical scattering processes are considered, the physical results do not depend on the choice of Floquet–Brillouin zone.

In the hypothetical absence of Floquet–Umklapp processes, all allowed scattering processes are akin to those of an equilibrium system and the steady state must therefore be of Floquet–Gibbs form[171]. Importantly, although some Floquet–Umklapp processes involve photon-assisted scattering that may be suppressed for weak driving, others are simply spontaneous processes that appear inverted owing to the folding of energies into the quasienergy Brillouin zone and cannot be neglected. For example, an electron near $\mathbf{k} = 0$ in the original conduction band can recombine with a nearby hole in the original valence band via the spontaneous emission of a photon. Due to the Floquet band inversion, this

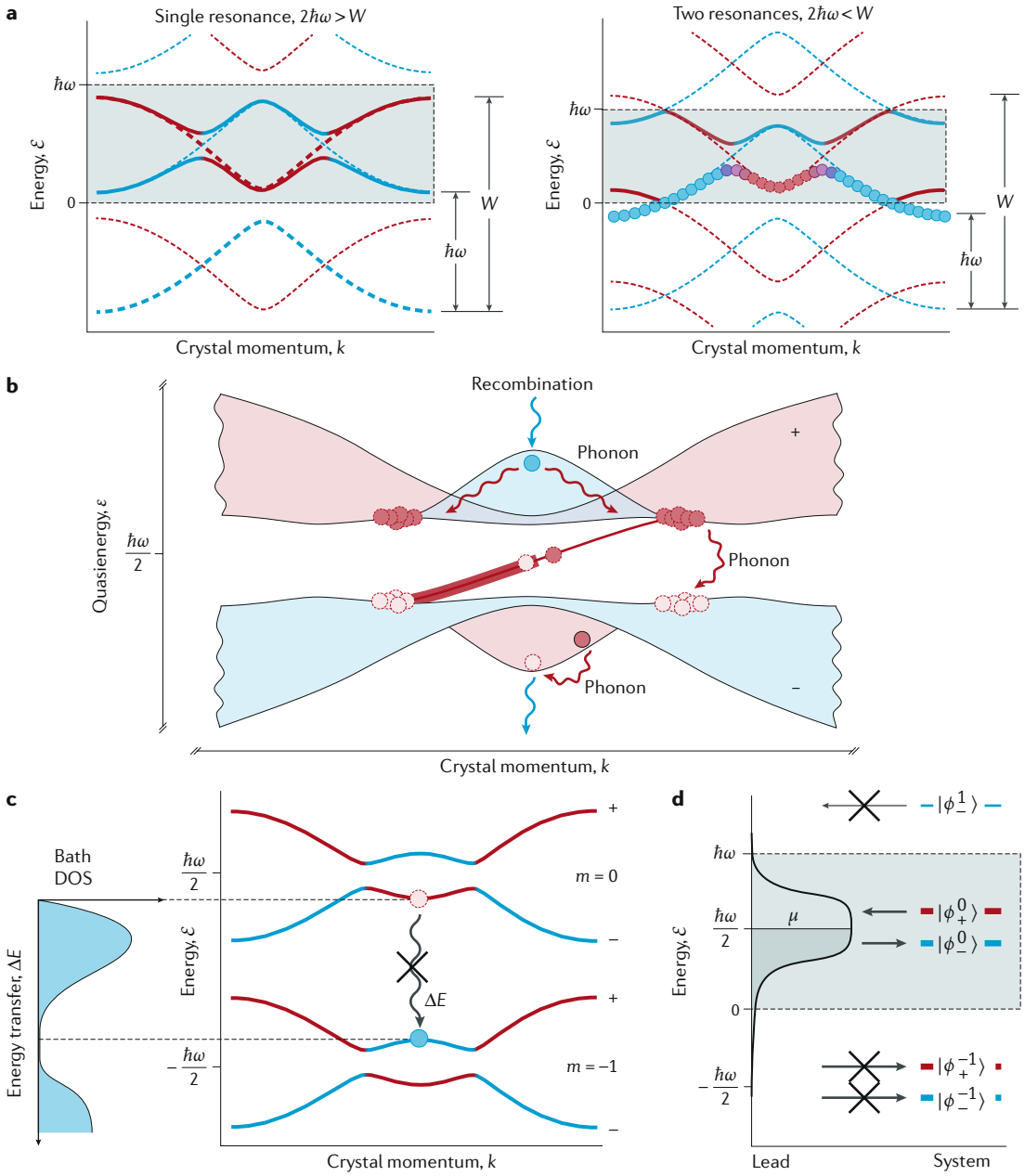

Fig. 5 | **Steady states of Floquet topological insulators coupled to external baths. a** | For $2\hbar\omega > W$, where $\hbar\omega$ is the driving frequency and W is the bandwidth (left), there are no two-photon (or higher-order) resonances, and the Floquet bands (solid lines) exhibit at most a single band inversion compared with the original bands (bold dotted lines). For $2\hbar\omega < W$ (right), the characters of the Floquet bands switch multiple times between valence-band-like (blue) and conduction-band-like (red). In the generalized Floquet insulator state, the bottom of the original valence band remains full and the top of the original conduction band remains empty, as indicated by the filled circles. **b** | Scattering processes stabilizing a Floquet insulator state with remnant electron and hole excitations (filled and empty circles, respectively). Excitations from the lower to the upper bulk Floquet band are produced by radiative recombination (blue wavy arrows), as well as Floquet–Umklapp phonon scattering and electron–electron collisions. Relaxation to the lower Floquet band is mediated predominantly by electron–phonon scattering (red wavy arrows). **c** | Reservoir engineering can suppress unwanted Floquet–Umklapp electron–phonon and electron–photon scattering by suppressing the corresponding densities of states (DOS) at relevant transition energies. As illustrated, the bath DOS is suppressed at the transition energy corresponding to the radiative recombination process indicated by the wavy arrow. The label m refers to the Floquet side band harmonics in the expansion of the Floquet states, see BOX 1. **d** | Coupling Floquet topological insulators to external electronic leads through energy filters suppresses photon-assisted tunnelling. In the absence of the filter, the population of a Floquet state with quasienergy ε is influenced by the populations of electrons in the reservoir at several energies $\varepsilon + n\hbar\omega$, where n takes integer values, through the sideband components $\{|\phi_{\pm}^{n}\rangle\}$, which can be both below and above the Fermi level in the lead. With an appropriate filter of bandwidth less than $\hbar\omega$, only one sideband component effectively participates and the population of a Floquet state is determined by electronic states in the lead at a single energy. As drawn, the Floquet states $|\psi_{-}\rangle$ and $|\psi_{+}\rangle$, with sideband components $\{|\phi_{\pm}^{n}\rangle\}$, will be filled and empty, respectively. Panel **c** adapted from REF.[169] CC BY 3.0.

process corresponds to the scattering of an electron from the lower Floquet band to the upper one (FIG. 5b). Such Floquet–Umklapp processes add excited electrons in the upper Floquet band and holes in the lower one. Once such excitations are created, they quickly relax to the local extrema of the Floquet bands by emitting acoustic phonons. Although acoustic phonons typically do not scatter electrons between the conduction and valence bands, the strong drive-induced hybridization of the bands near the resonances allows electrons to traverse the Floquet gap to recombine with holes in the lower Floquet band via further acoustic phonon emission.

When the timescale for Floquet–Umklapp scattering is much longer than the timescale for phonon-assisted cooling, the steady state resembles the generalized Floquet insulator state. However, due to Floquet–Umklapp scattering, the steady state exhibits small additional pockets of electron and hole excitations in the upper and lower Floquet bands, respectively. Deviations from the Floquet insulator state lead to deviations of the period-averaged d.c. Hall conductivity $\bar{\sigma}_{xy}(\Omega = 0)$ from a quantized value in units of e^2/h (REFS[158,160,172]).

By engineering the environment of an FTI, deviations from the desired steady state can be minimized. Floquet–Umklapp scattering involving photon or phonon emission can be inhibited by suppressing the densities of states of these bosonic modes at appropriate energies[168,169] (FIG. 5c). For example, a cavity can be used to suppress the density of states of the electromagnetic environment at the frequencies corresponding to electron–hole recombination near $\mathbf{k} = 0$.

The need for reservoir engineering is even more pronounced when electronic reservoirs are connected to the system. For conventional metallic contacts with a wide bandwidth, electrons (holes) in the contact with energies well below (above) the Fermi level may tunnel into the upper (lower) Floquet bands via absorption of integer multiples of $\hbar\omega$ from the drive. These processes lead to a proliferation of excitations with respect to the ideal Floquet insulator[160,168,169]. An energy-selective filter placed between the contact and the FTI suppresses the tunnelling density of states outside a narrow window defined by the filter (FIG. 5d). Such a filter not only suppresses unwanted tunnelling events but also depletes the number of excitations and helps to establish and control a sharp Fermi level in the FTI's edge states[160,168].

The considerations outlined here provide a framework for identifying promising setups for realizing steady-state FTIs in solid-state systems. The next important steps on the horizon are to find specific candidate materials and compatible implementations of the bath engineering schemes discussed above. Theoretically, the role of higher-order resonances and their impact on transport coefficients also remain to be elucidated.

Outlook

Floquet engineering provides a versatile set of tools for controlling topological properties of quantum matter. Experiments in solid-state, optical and cold atomic systems have demonstrated many of the basic features of topological Floquet band engineering at the single-particle level. Important ingredients for Floquet engineering of many-body systems, including Floquet MBL[140] and drive-tunable exchange interactions[22], have been experimentally demonstrated with cold atoms. These encouraging early works highlight the promise of Floquet engineering, and point to a number of important open theoretical and experimental challenges.

One of the key hallmarks of topological behaviour in equilibrium electronic systems, and an important motivation in Floquet engineering, is the appearance of robustly quantized observables, such as transport coefficients. On a theoretical level, it is therefore important to investigate the degree of robustness and quantization that can be achieved for observables in non-equilibrium topological matter. In the context of the transient regime, an important question is how to optimize the preparation of desired quasisteady (prethermal) states. To achieve this goal through the design of appropriate driving protocols, efficient methods for computing the prethermal Hamiltonian H_* are needed. New approaches for obtaining long prethermal time windows, in particular, accounting for the presence of coupling to external baths, may open new possibilities for Floquet engineering. The transient and MBL regimes may host intriguing new strongly correlated anomalous phases that remain to be discovered. Identifying promising new candidate materials and setups where reservoir engineering can be achieved, and devising new strategies for obtaining stable topological phases in the steady states of interacting systems are also crucial for further progress in the field. Furthermore, the roles of multiple resonances in determining steady-state properties are important questions to be addressed. Experimentally, stabilizing topological steady or prethermal states and observing robust quantization of observables in many-body systems remain open challenges and prominent goals in the field. Going beyond the realm of FTIs, we anticipate that Floquet engineering of stable strongly correlated and topologically ordered phases of matter will play an important role in future progress in contemporary condensed-matter physics and quantum information.

Published online: 04 May 2020

1. Basov, D. N., Averitt, R. D. & Hsieh, D. Towards properties on demand in quantum materials. *Nat. Mater.* **16**, 1077–1088 (2017).
2. Floquet, G. Sur les equations differentielles lineaires a coefficients periodiques. *Ann. Ecole Norm. Superieure* **12**, 47–88 (1883).
3. Jaksch, D. & Zoller, P. Creation of effective magnetic fields in optical lattices: the Hofstadter butterfly for cold neutral atoms. *New J. Phys.* **5**, 56.1–56.11 (2003).
4. Mueller, E. J. Artificial electromagnetism for neutral atoms: escher staircase and Laughlin liquids. *Phys. Rev. A* **70**, 041603 (2004).
5. Sørensen, A. S., Demler, E. & Lukin, M. D. Fractional quantum Hall states of atoms in optical lattices. *Phys. Rev. Lett.* **94**, 086803 (2005).
6. Yao, W., MacDonald, A. H. & Niu, Q. Optical control of topological quantum transport in semiconductors. *Phys. Rev. Lett.* **99**, 047401 (2007).
7. Hasan, M. Z. & Kane, C. L. Colloquium: topological insulators. *Rev. Mod. Phys.* **82**, 3045–3067 (2010).
8. Oka, T. & Aoki, H. Photovoltaic Hall effect in graphene. *Phys. Rev. B* **79**, 081406 (2009).
9. Kitagawa, T., Berg, E., Rudner, M. & Demler, E. Topological characterization of periodically driven quantum systems. *Phys. Rev. B* **82**, 235114 (2010).
10. Lindner, N. H., Refael, G. & Galitski, V. Floquet topological insulator in semiconductor quantum wells. *Nat. Phys.* **7**, 490–495 (2011).
11. D'Alessio, L. & Rigol, M. Long-time behavior of isolated periodically driven interacting lattice systems. *Phys. Rev. X* **4**, 041048 (2014).
12. Lazarides, A., Das, A. & Moessner, R. Equilibrium states of generic quantum systems subject to periodic driving. *Phys. Rev. E* **90**, 012110 (2014).
13. Prosen, T. Time evolution of a quantum many-body system: transition from integrability to ergodicity in the thermodynamic limit. *Phys. Rev. Lett.* **80**, 1808 (1998).

14. Kukuljan, I. & Prosen, T. Corner transfer matrices for 2D strongly coupled many-body Floquet systems. *J. Stat. Mech.* **2016**, 043305 (2016).
15. Citro, R. et al. Dynamical stability of a many-body Kapitza pendulum. *Ann. Phys.* **360**, 694–710 (2015).
16. Chandran, A. & Sondhi, S. L. Interaction-stabilized steady states in the driven *O*(*N*) model. *Phys. Rev. B* **93**, 174305 (2016).
17. Haldar, A., Moessner, R. & Das, A. Onset of Floquet thermalization. *Phys. Rev. B* **97**, 245122 (2018).
18. Seetharam, K., Titum, P., Kolodrubetz, M. & Refael, G. Absence of thermalization in finite isolated interacting Floquet systems. *Phys. Rev. B* **97**, 014311 (2018).
19. Grushin, A. G., Gómez-León, Á. & Neupert, T. Floquet fractional Chern insulators. *Phys. Rev. Lett.* **112**, 156801 (2014).
20. Klinovaja, J., Stano, P. & Loss, D. Topological floquet phases in driven coupled Rashba nanowires. *Phys. Rev. Lett.* **116**, 176401 (2016).
21. Liu, J., Hejazi, K. & Balents, L. Floquet engineering of multiorbital Mott insulators: applications to orthorhombic titanates. *Phys. Rev. Lett.* **121**, 107201 (2018).
22. Görg, F. et al. Enhancement and sign change of magnetic correlations in a driven quantum many-body system. *Nature* **553**, 481–485 (2018).
23. Kennes, D. M., de la Torre, A., Ron, A., Hsieh, D. & Millis, A. J. Floquet engineering in quantum chains. *Phys. Rev. Lett.* **120**, 127601 (2018).
24. Rudner, M. S., Lindner, N. H., Berg, E. & Levin, M. Anomalous edge states and the bulk-edge correspondence for periodically driven two-dimensional systems. *Phys. Rev. X* **3**, 031005 (2013).
25. Nathan, F. & Rudner, M. S. Topological singularities and the general classification of Floquet–Bloch systems. *New J. Phys.* **17**, 125014 (2015).
26. Roy, R. & Harper, F. Floquet topological phases with symmetry in all dimensions. *Phys. Rev. B* **95**, 195128 (2017).
27. Roy, R. & Harper, F. Periodic table for Floquet topological insulators. *Phys. Rev. B* **96**, 155118 (2017).
28. Yao, S., Yan, Z. & Wang, Z. Topological invariants of Floquet systems: general formulation, special properties, and Floquet topological defects. *Phys. Rev. B* **96**, 195303 (2017).
29. Gómez-León, A. & Platero, G. Floquet–Bloch theory and topology in periodically driven lattices. *Phys. Rev. Lett.* **110**, 200403 (2013).
30. Graf, G. M. & Tauber, C. Bulk-edge correspondence for two-dimensional Floquet topological insulators. *Ann. Henri Poincare* **19**, 709–741 (2018).
31. Shapiro, J. & Tauber, C. Strongly disordered Floquet topological systems. *Ann. Henri Poincare* **20**, 1837–1875 (2019).
32. Khemani, V., Lazarides, A., Moessner, R. & Sondhi, S. L. Phase structure of driven quantum systems. *Phys. Rev. Lett.* **116**, 250401 (2016).
33. Else, D. V., Bauer, B. & Nayak, C. Floquet time crystals. *Phys. Rev. Lett.* **117**, 090402 (2016).
34. Else, D. V., Bauer, B. & Nayak, C. Prethermal phases of matter protected by time-translation symmetry. *Phys. Rev. X* **7**, 011026 (2017).
35. Rudner, M. S. & Song, J. C. W. Self-induced Berry flux and spontaneous non-equilibrium magnetism. *Nat. Phys.* **15**, 1017–1021 (2019).
36. Nag, T., Slager, R.-J., Higuchi, T. & Oka, T. Dynamical synchronization transition in interacting electron systems. *Phys. Rev. B* **100**, 134301 (2019).
37. Kinoshita, S., Murata, K. & Oka, T. Holographic floquet states II: Floquet condensation of vector mesons in nonequilibrium phase diagram. *J. High Energy Phys.* **2018**, 96 (2018).
38. Harper, F., Roy, R., Rudner, M. S. & Sondhi, S. Topology and broken symmetry in Floquet systems. *Annu. Rev. Condens. Matter Phys.* **11**, 345–368 (2020).
39. von Keyserlingk, C. W. & Sondhi, S. L. Phase structure of one-dimensional interacting Floquet systems. I. Abelian symmetry-protected topological phases. *Phys. Rev. B* **93**, 245145 (2016).
40. Potter, A. C., Morimoto, T. & Vishwanath, A. Classification of interacting topological Floquet phases in one dimension. *Phys. Rev. X* **6**, 041001 (2016).
41. Else, D. V. & Nayak, C. Classification of topological phases in periodically driven interacting systems. *Phys. Rev. B* **93**, 201103 (2016).
42. Harper, F. & Roy, R. Floquet topological order in interacting systems of bosons and fermions. *Phys. Rev. Lett.* **118**, 115301 (2017).
43. Moessner, R. & Sondhi, S. L. Equilibration and order in quantum Floquet matter. *Nat. Phys.* **13**, 424–428 (2017).
44. Eckardt, A. Colloquium: atomic quantum gases in periodically driven optical lattices. *Rev. Mod. Phys.* **89**, 011004 (2017).
45. Cooper, N. R., Dalibard, J. & Spielman, I. B. Topological bands for ultracold atoms. *Rev. Mod. Phys.* **91**, 015005 (2019).
46. Ozawa, T. et al. Topological photonics. *Rev. Mod. Phys.* **91**, 015006 (2019).
47. Wang, Y. H., Steinberg, H., Jarillo-Herrero, P. & Gedik, N. Observation of Floquet–Bloch states on the surface of a topological insulator. *Science* **342**, 453–457 (2013).
48. McIver, J. W. et al. Light-induced anomalous Hall effect in graphene. *Nat. Phys.* **16**, 38–41 (2019).
49. Rudner, M. S. & Lindner, N. H. The Floquet engineer's handbook. Preprint at https://arxiv.org/abs/2003.08252 (2020).
50. Xiao, D., Chang, M.-C. & Niu, Q. Berry phase effects on electronic properties. *Rev. Mod. Phys.* **82**, 1959–2007 (2010).
51. Kitagawa, T., Oka, T., Brataas, A., Fu, L. & Demler, E. Transport properties of nonequilibrium systems under the application of light: photoinduced quantum Hall insulators without Landau levels. *Phys. Rev. B* **84**, 235108 (2011).
52. Lindner, N. H., Bergman, D. L., Refael, G. & Galitski, V. Topological Floquet spectrum in three dimensions via a two-photon resonance. *Phys. Rev. B* **87**, 235131 (2013).
53. Sie, E. J. et al. Valley-selective optical Stark effect in monolayer WS_2. *Nat. Mater.* **14**, 290–294 (2015).
54. Usaj, G., Perez-Piskunow, P. M., Foa Torres, L. E. F. & Balseiro, C. A. Irradiated graphene as a tunable Floquet topological insulator. *Phys. Rev. B* **90**, 115423 (2014).
55. Kundu, A., Fertig, H. A. & Seradjeh, B. Effective theory of Floquet topological transitions. *Phys. Rev. Lett.* **113**, 236803 (2014).
56. Quelle, A., Goerbig, M. O. & Smith, C. M. Bandwidth-resonant Floquet states in honeycomb optical lattices. *New J. Phys.* **18**, 015006 (2016).
57. Gu, Z., Fertig, H. A., Arovas, D. P. & Auerbach, A. Floquet spectrum and transport through an irradiated graphene ribbon. *Phys. Rev. Lett.* **107**, 216601 (2011).
58. Rodriguez-Vega, M. & Seradjeh, B. Universal fluctuations of Floquet topological invariants at low frequencies. *Phys. Rev. Lett.* **121**, 036402 (2018).
59. Delplace, P., Gómez-León, A. & Platero, G. Merging of Dirac points and Floquet topological transitions in ac-driven graphene. *Phys. Rev. B* **88**, 245422 (2013).
60. Sentef, M. A. et al. Theory of Floquet band formation and local pseudospin textures in pump–probe photoemission of graphene. *Nat. Commun.* **6**, 7047 (2015).
61. Iadecola, T. et al. Materials design from nonequilibrium steady states: driven graphene as a tunable semiconductor with topological properties. *Phys. Rev. Lett.* **110**, 176603 (2013).
62. Jiang, L. et al. Majorana fermions in equilibrium and in driven cold-atom quantum wires. *Phys. Rev. Lett.* **106**, 220402 (2011).
63. Thakurathi, M., Loss, D. & Klinovaja, J. Floquet Majorana fermions and parafermions in driven Rashba nanowires. *Phys. Rev. B* **95**, 155407 (2017).
64. Kennes, D. M. et al. Chiral one-dimensional Floquet topological insulators beyond the rotating wave approximation. *Phys. Rev. B* **100**, 041103 (2019).
65. Wang, R., Wang, B., Shen, R., Sheng, L. & Xing, D. Y. Floquet Weyl semimetal induced by off-resonant light. *Europhys. Lett.* **105**, 17004 (2014).
66. Chan, C.-K., Lee, P. A., Burch, K. S., Han, J. H. & Ran, Y. When chiral photons meet chiral fermions: photoinduced anomalous Hall effects in Weyl semimetals. *Phys. Rev. Lett.* **116**, 026805 (2016).
67. Chan, C.-K., Oh, Y.-T., Han, J. H. & Lee, P. A. Type-II Weyl cone transitions in driven semimetals. *Phys. Rev. B* **94**, 121106 (2016).
68. Hübener, H., Sentef, M. A., de Giovannini, U., Kemper, A. F. & Rubio, A. Creating stable Floquet–Weyl semimetals by laser-driving of 3D Dirac materials. *Nat. Commun.* **8**, 13940 (2017).
69. Fleury, R., Khanikev, A. B. & Alu, A. Floquet topological insulators for sound. *Nat. Commun.* **7**, 11744 (2016).
70. Dalibard, J., Gerbier, F., Juzeliūnas, G. & Öhberg, P. Colloquium: artificial gauge potentials for neutral atoms. *Rev. Mod. Phys.* **83**, 1523–1543 (2011).
71. Goldman, N., Juzeliunas, G., Ohberg, P. & Spielman, I. B. Light-induced gauge fields for ultracold atoms. *Rep. Prog. Phys.* **77**, 126401 (2014).
72. Kitaev, A. Periodic table for topological insulators and superconductors. *AIP Conf. Proc.* **1134**, 22–30 (2009).
73. Ryu, S., Schnyder, A. P., Furusaki, A. & Ludwig, A. W. W. Topological insulators and superconductors: tenfold way and dimensional hierarchy. *New J. Phys.* **12**, 065010 (2010).
74. Thouless, D. J. Quantization of particle transport. *Phys. Rev. B* **27**, 6083 (1983).
75. Gross, D., Nesme, V., Vogts, H. & Werner, R. F. Index theory of one dimensional quantum walks and cellular automata. *Commun. Math. Phys.* **310**, 419–454 (2012).
76. Higashikawa, S., Nakagawa, M. & Ueda, M. Floquet chiral magnetic effect. *Phys. Rev. Lett.* **123**, 066403 (2019).
77. Sun, X.-Q., Xiao, M., Bzdušek, Tcv, Zhang, S.-C. & Fan, S. Three-dimensional chiral lattice fermion in Floquet systems. *Phys. Rev. Lett.* **121**, 196401 (2018).
78. Bernevig, B. A., Hughes, T. L. & Zhang, S.-C. Quantum spin Hall effect and topological phase transition in HgTe quantum wells. *Science* **314**, 1757–1761 (2006).
79. Halperin, B. I. Quantized Hall conductance, current-carrying edge states, and the existence of extended states in a two-dimensional disordered potential. *Phys. Rev. B* **25**, 2185–2190 (1982).
80. Hatsugai, Y. Chern number and edge states in the integer quantum Hall effect. *Phys. Rev. Lett.* **71**, 3697 (1993).
81. Carpentier, D., Delplace, P., Fruchart, M. & Gawedzki, K. Topological index for periodically driven time-reversal invariant 2D systems. *Phys. Rev. Lett.* **114**, 106806 (2015).
82. Broome, M. A. et al. Discrete single-photon quantum walks with tunable decoherence. *Phys. Rev. Lett.* **104**, 153602 (2010).
83. Rechtsman, M. C. et al. Photonic Floquet topological insulators. *Nature* **496**, 196–200 (2013).
84. Hu, W. et al. Measurement of a topological edge invariant in a microwave network. *Phys. Rev. X* **5**, 011012 (2015).
85. Cheng, Q. et al. Observation of anomalous π modes in photonic Floquet engineering. *Phys. Rev. Lett.* **122**, 173901 (2019).
86. Mukherjee, S. et al. Experimental observation of anomalous topological edge modes in a slowly-driven photonic lattice. *Nat. Commun.* **8**, 13918 (2017).
87. Maczewsky, L. J., Zeuner, J. M., Nolte, S. & Szameit, A. Observation of photonic anomalous Floquet topological insulators. *Nat. Commun.* **8**, 13756 (2017).
88. Nakajima, S. et al. Topological Thouless pumping of ultracold fermions. *Nat. Phys.* **12**, 296–300 (2016).
89. Lohse, M., Schweizer, C., Zilberberg, O., Aidelsburger, M. & Bloch, I. A Thouless quantum pump with ultracold bosonic atoms in an optical superlattice. *Nat. Phys.* **12**, 350–354 (2016).
90. Reichl, M. D. & Mueller, E. J. Floquet edge states with ultracold atoms. *Phys. Rev. A* **89**, 063628 (2014).
91. Quelle, A., Weitenberg, C., Sengstock, K. & Morais Smith, C. Driving protocol for a Floquet topological phase without static counterpart. *New J. Phys.* **19**, 113010 (2017).
92. Liu, D. T., Shabani, J. & Mitra, A. Floquet Majorana zero and π modes in planar Josephson junctions. *Phys. Rev. B* **99**, 094303 (2019).
93. Kundu, A. & Seradjeh, B. Transport signatures of Floquet Majorana fermions in driven topological superconductors. *Phys. Rev. Lett.* **111**, 136402 (2013).
94. Foa Torres, L. E. F., Perez-Piskunow, P. M., Balseiro, C. A. & Usaj, G. Multiterminal conductance of a Floquet topological insulator. *Phys. Rev. Lett.* **113**, 266801 (2014).
95. Farrell, A. & Pereg-Barnea, T. Photon-inhibited topological transport in quantum well heterostructures. *Phys. Rev. Lett.* **115**, 106403 (2015).
96. Farrell, A. & Pereg-Barnea, T. Edge-state transport in Floquet topological insulators. *Phys. Rev. B* **93**, 045121 (2016).
97. Kundu, A., Rudner, M. S., Berg, E. & Lindner, N. H. Quantized large-bias current in the anomalous Floquet–Anderson insulator. *Phys. Rev. B* **101**, 041403(R) (2020).
98. Salerno, G. et al. Quantized Hall conductance of a single atomic wire: a proposal based on synthetic dimensions. *Phys. Rev. X* **9**, 041001 (2019).
99. Kohler, S., Lehmann, J. & Hanggi, P. Driven quantum transport on the nanoscale. *Phys. Rep.* **406**, 379–443 (2005).

100. Perez-Piskunow, P. M., Foa Torres, L. E. F. & Usaj, G. Hierarchy of Floquet gaps and edge states for driven honeycomb lattices. *Phys. Rev. A* **91**, 043625 (2015).
101. Uhrig, G. S., Kalthoff, M. H. & Freericks, J. K. Positivity of the spectral densities of retarded Floquet Green functions. *Phys. Rev. Lett.* **122**, 130604 (2019).
102. Sengupta, K., Žutić, I., Kwon, H.-J., Yakovenko, V. M. & Das Sarma, S. Midgap edge states and pairing symmetry of quasi-one-dimensional organic superconductors. *Phys. Rev. B* **63**, 144531 (2001).
103. Law, K. T., Lee, P. A. & Ng, T. K. Majorana fermion induced resonant Andreev reflection. *Phys. Rev. Lett.* **103**, 237001 (2009).
104. Titum, P., Berg, E., Rudner, M. S., Refael, G. & Lindner, N. H. Anomalous Floquet–Anderson insulator as a nonadiabatic quantized charge pump. *Phys. Rev. X* **6**, 021013 (2016).
105. Dahlhaus, J. P., Fregoso, B. M. & Moore, J. E. Magnetization signatures of light-induced quantum Hall edge states. *Phys. Rev. Lett.* **114**, 246802 (2015).
106. Nathan, F., Rudner, M. S., Lindner, N. H., Berg, E. & Refael, G. Quantized magnetization density in periodically driven systems. *Phys. Rev. Lett.* **119**, 186801 (2017).
107. Mahmood, F. et al. Selective scattering between Floquet–Bloch and Volkov states in a topological insulator. *Nat. Phys.* **12**, 306–310 (2016).
108. Fregoso, B. M., Wang, Y. H., Gedik, N. & Galitski, V. Driven electronic states at the surface of a topological insulator. *Phys. Rev. B* **88**, 155129 (2013).
109. Farrell, A., Arsenault, A. & Pereg-Barnea, T. Dirac cones, Floquet side bands, and theory of time-resolved angle-resolved photoemission. *Phys. Rev. B* **94**, 155304 (2016).
110. Kandelaki, E. & Rudner, M. S. Many-body dynamics and gap opening in interacting periodically driven systems. *Phys. Rev. Lett.* **121**, 036801 (2018).
111. Jotzu, G. et al. Experimental realization of the topological Haldane model with ultracold fermions. *Nature* **515**, 237–240 (2014).
112. Aidelsburger, M. et al. Measuring the Chern number of Hofstadter bands with ultracold bosonic atoms. *Nat. Phys.* **11**, 162–166 (2015).
113. Flaschner, N. et al. Experimental reconstruction of the Berry curvature in a Floquet Bloch band. *Science* **352**, 1091–1094 (2016).
114. Flaschner, N. et al. Observation of dynamical vortices after quenches in a system with topology. *Nat. Phys.* **14**, 265–268 (2018).
115. Tarnowski, M. et al. Measuring topology from dynamics by obtaining the Chern number from a linking number. *Nat. Commun.* **10**, 1728 (2019).
116. Asteria, L. et al. Measuring quantized circular dichroism in ultracold topological matter. *Nat. Phys.* **15**, 449–454 (2019).
117. Bukov, M., D'Alessio, L. & Polkovnikov, A. Universal high-frequency behavior of periodically driven systems: from dynamical stabilization to Floquet engineering. *Adv. Phys.* **64**, 139–226 (2015).
118. Eckardt, A. & Anisimovas, E. High-frequency approximation for periodically driven quantum systems from a Floquet-space perspective. *New J. Phys.* **17**, 093039 (2015).
119. Kuwahara, T., Mori, T. & Saito, K. Floquet–Magnus theory and generic transient dynamics in periodically driven many-body quantum systems. *Ann. Phys.* **367**, 96–124 (2016).
120. Abanin, D. A., De Roeck, W., Ho, W. W. & Huveneers, F. Effective Hamiltonians, prethermalization, and slow energy absorption in periodically driven many-body systems. *Phys. Rev. B* **95**, 014112 (2017).
121. Lindner, N. H., Berg, E. & Rudner, M. S. Universal Chiral quasisteady states in periodically driven many-body systems. *Phys. Rev. X* **7**, 011018 (2017).
122. Mori, T., Ikeda, T. N., Kamanishi, E. & Ueda, M. Thermalization and prethermalization in isolated quantum systems: a theoretical overview. *J. Phys. B* **51**, 112001 (2018).
123. Bukov, M., Heyl, M., Huse, D. A. & Polkovnikov, A. Heating and many-body resonances in a periodically driven two-band system. *Phys. Rev. B* **93**, 155132 (2016).
124. Abanin, D. A., De Roeck, W. & Huveneers, F. Exponentially slow heating in periodically driven many-body systems. *Phys. Rev. Lett.* **115**, 256803 (2015).
125. Bilitewski, T. & Cooper, N. R. Scattering theory for Floquet–Bloch states. *Phys. Rev. A* **91**, 033601 (2015).
126. Reitter, M. et al. Interaction dependent heating and atom loss in a periodically driven optical lattice. *Phys. Rev. Lett.* **119**, 200402 (2017).
127. Abanin, D., De Roeck, W., Ho, W. W. & Huveneers, F. A rigorous theory of many-body prethermalization for periodically driven and closed quantum systems. *Commun. Math. Phys.* **354**, 809–827 (2017).
128. Mori, T. Floquet prethermalization in periodically driven classical spin systems. *Phys. Rev. B* **98**, 104303 (2018).
129. Howell, O., Weinberg, P., Sels, D., Polkovnikov, A. & Bukov, M. Asymptotic prethermalization in periodically driven classical spin chains. *Phys. Rev. Lett.* **122**, 010602 (2019).
130. Vogl, M., Laurell, P., Barr, A. D. & Fiete, G. A. Flow equation approach to periodically driven quantum systems. *Phys. Rev. X* **9**, 021037 (2019).
131. Regnault, N. & Bernevig, B. A. Fractional Chern insulator. *Phys. Rev. X* **1**, 021014 (2011).
132. Claassen, M., Jiang, H.-C., Mortiz, B. & Devereaux, T. P. Dynamical time-reversal symmetry breaking and photo-induced chiral spin liquids in frustrated mott insulators. *Nat. Commun.* **8**, 1192 (2017).
133. Liu, J., Hejazi, K. & Balents, L. Floquet engineering of multiorbital Mott insulators: applications to orthorhombic titanates. *Phys. Rev. Lett.* **121**, 107201 (2018).
134. Basko, D. M., Aleiner, I. L. & Altshuler, B. L. Metal insulator transition in a weakly interacting many-electron system with localized single-particle states. *Ann. Phys.* **321**, 1126–1205 (2006).
135. Oganesyan, V. & Huse, D. A. Localization of interacting fermions at high temperature. *Phys. Rev. B* **75**, 155111 (2007).
136. Pal, A. & Huse, D. A. Many-body localization phase transition. *Phys. Rev. B* **82**, 174411 (2010).
137. Nandkishore, R. & Huse, D. A. Many-body localization and thermalization in quantum statistical mechanics. *Annu. Rev. Condens. Matter Phys.* **6**, 15–38 (2015).
138. Lazarides, A., Das, A. & Moessner, R. Fate of many-body localization under periodic driving. *Phys. Rev. Lett.* **115**, 030402 (2015).
139. Ponte, P., Papić, Z., Huveneers, F. & Abanin, D. A. Many-body localization in periodically driven systems. *Phys. Rev. Lett.* **114**, 140401 (2015).
140. Bordia, P., Luschen, H., Schneider, U., Knap, M. & Bloch, I. Periodically driving a many-body localized quantum system. *Nat. Phys.* **13**, 460–464 (2017).
141. Wilczek, F. Quantum time crystals. *Phys. Rev. Lett.* **109**, 160401 (2012).
142. Zeng, T.-S. & Sheng, D. N. Prethermal time crystals in a one-dimensional periodically driven Floquet system. *Phys. Rev. B* **96**, 094202 (2017).
143. Zhang, J. et al. Observation of a discrete time crystal. *Nature* **543**, 217–220 (2017).
144. Choi, S. et al. Observation of discrete time-crystalline order in a disordered dipolar many-body system. *Nature* **543**, 221–225 (2017).
145. Dykman, M. I., Bruder, C., Lörch, N. & Zhang, Y. Interaction-induced time-symmetry breaking in driven quantum oscillators. *Phys. Rev. B* **98**, 195444 (2018).
146. Nandkishore, R. & Potter, A. C. Marginal Anderson localization and many-body delocalization. *Phys. Rev. B* **90**, 195115 (2014).
147. Po, H. C., Fidkowski, L., Morimoto, T., Potter, A. C. & Vishwanath, A. Chiral Floquet phases of many-body localized bosons. *Phys. Rev. X* **6**, 041070 (2016).
148. Po, H. C., Fidkowski, L., Vishwanath, A. & Potter, A. C. Radical chiral Floquet phases in a periodically driven Kitaev model and beyond. *Phys. Rev. B* **96**, 245116 (2017).
149. Nathan, F., Abanin, D., Berg, E., Lindner, N. H. & Rudner, M. S. Anomalous Floquet insulators. *Phys. Rev. B* **99**, 195133 (2019).
150. Liu, D. E. Classification of the Floquet statistical distribution for time-periodic open systems. *Phys. Rev. B* **91**, 144301 (2015).
151. Shirai, T., Mori, T. & Miyashita, S. Condition for emergence of the Floquet–Gibbs state in periodically driven open systems. *Phys. Rev. E* **91**, 030101(R) (2015).
152. Shirai, T. et al. Effective Floquet–Gibbs states for dissipative quantum systems. *New J. Phys.* **18**, 053008 (2016).
153. Torres, M. & Kunold, A. Kubo formula for floquet states and photoconductivity oscillations in a two-dimensional electron gas. *Phys. Rev. B* **71**, 115313 (2005).
154. Mahan, G. D. *Many-Particle Physics* (Springer, 2000).
155. Kohn, W. Periodic thermodynamics. *J. Stat. Phys.* **103**, 417–423 (2001).
156. Hone, D. W., Ketzmerick, R. & Kohn, W. Time-dependent Floquet theory and absence of an adiabatic limit. *Phys. Rev. A* **56**, 4045 (1997).
157. Hone, D. W., Ketzmerick, R. & Kohn, W. Statistical mechanics of Floquet systems: the pervasive problem of near degeneracies. *Phys. Rev. E* **79**, 051129 (2009).
158. Dehghani, H., Oka, T. & Mitra, A. Out-of-equilibrium electrons and the Hall conductance of a Floquet topological insulator. *Phys. Rev. B* **91**, 155422 (2015).
159. Genske, M. & Rosch, A. Floquet–Boltzmann equation for periodically driven Fermi systems. *Phys. Rev. A* **92**, 062108 (2015).
160. Esin, I., Rudner, M. S., Refael, G. & Lindner, N. H. Quantized transport and steady states of Floquet topological insulators. *Phys. Rev. B* **97**, 245401 (2018).
161. Goebel, E. O. & Hildebrand, O. Thermalization of the electron–hole plasma in GaAs. *Phys. Stat. Sol.* **88**, 645–652 (1978).
162. Glazman, L. I. Resonant excitation of carriers in a semiconductor by a high-power laser pulse. *Sov. Phys. JETP* **53**, 178–181 (1981).
163. Glazman, L. I. Kinetics of electrons and holes in direct gap semiconductors photoexcited by high intensity pulses. *Sov. Phys. Semi* **17**, 494–498 (1983).
164. Chow, W. W. & Koch, S. W. *Semiconductor-Laser Fundamentals* (Springer, 1999).
165. Huang, M. H. et al. Room-temperature ultraviolet nanowire nanolasers. *Science* **292**, 1897–1899 (2001).
166. Röder, R. et al. Continuous wave nanowire lasing. *Nano Lett.* **13**, 3602–3606 (2013).
167. Dehghani, H., Oka, T. & Mitra, A. Dissipative Floquet topological systems. *Phys. Rev. B* **90**, 195429 (2014).
168. Seetharam, K. I., Bardyn, C.-E., Lindner, N. H., Rudner, M. S. & Refael, G. Controlled population of Floquet–Bloch states via coupling to Bose and Fermi baths. *Phys. Rev. X* **5**, 041050 (2015).
169. Iadecola, T., Neupert, T. & Chamon, C. Occupation of topological Floquet bands in open systems. *Phys. Rev. B* **91**, 235133 (2015).
170. Dykman, M. I., Marthaler, M. & Peano, V. Quantum heating of a parametrically modulated oscillator: spectral signatures. *Phys. Rev. A* **83**, 052115 (2011).
171. Galitskii, V. M., Goreslavskii, S. P. & Elesin, V. F. Electric and magnetic properties of a semiconductor in the field of a strong electromagnetic wave. *Sov. Phys. JETP* **30**, 117–122 (1970).
172. Sato, S. A. et al. Microscopic theory for the light-induced anomalous Hall effect in graphene. *Phys. Rev. B* **99**, 214302 (2019).
173. Singh, K. et al. Quantifying and controlling prethermal nonergodicity in interacting Floquet matter. *Phys. Rev. X* **9**, 041021 (2019).
174. Holthaus, M. Floquet engineering with quasienergy bands of periodically driven optical lattices. *J. Phys. B* **49**, 013001 (2016).
175. Altland, A. & Zirnbauer, M. R. Nonstandard symmetry classes in mesoscopic normal-superconducting hybrid structures. *Phys. Rev. B* **55**, 1142 (1997).
176. Asbóth, J. K. & Obuse, H. Bulk-boundary correspondence for chiral symmetric quantum walks. *Phys. Rev. B* **88**, 121406 (2013).
177. Asbóth, J. K., Tarasinski, B. & Delplace, P. Chiral symmetry and bulk-boundary correspondence in periodically driven one-dimensional systems. *Phys. Rev. B* **90**, 125143 (2014).
178. Lababidi, M., Satija, I. I. & Zhao, E. Counter-propagating edge modes and topological phases of a kicked quantum Hall system. *Phys. Rev. Lett.* **112**, 026805 (2014).
179. Zhou, Z., Satija, I. I. & Zhao, E. Floquet edge states in a harmonically driven integer quantum Hall system. *Phys. Rev. B* **90**, 205108 (2014).
180. Yao, S., Yan, Z. & Wang, Z. Topological invariants of Floquet systems: general formulation, special properties, and Floquet topological defects. *Phys. Rev. B* **96**, 195303 (2017).
181. de Gennes, P. G. *Superconductivity of Metals and Alloys* (Springer, 2000).
182. Morimoto, T., Po, H. C. & Vishwanath, A. Floquet topological phases protected by time glide symmetry. *Phys. Rev. B* **95**, 195155 (2017).

183. Xu, S. & Wu, C. Space-time crystal and space-time group. *Phys. Rev. Lett.* **120**, 096401 (2018).
184. Peng, Y. & Refael, G. Floquet second-order topological insulators from nonsymmorphic space-time symmetries. *Phys. Rev. Lett.* **123**, 016806 (2019).
185. Liu, D. E., Levchenko, A. & Baranger, H. U. Floquet Majorana fermions for topological qubits in superconducting devices and cold-atom systems. *Phys. Rev. Lett.* **111**, 047002 (2013).
186. Dal Lago, V., Atala, M. & Foa Torres, L. E. F. Floquet topological transitions in a driven one-dimensional topological insulator. *Phys. Rev. A* **92**, 023624 (2015).
187. Bauer, B. et al. Topologically protected braiding in a single wire using Floquet Majorana modes. *Phys. Rev. B* **100**, 041102 (2019).

Acknowledgements
The authors thank all of their collaborators on FTI-related work, with whom they have had many stimulating interactions. In particular, they acknowledge E. Berg, E. Demler, V. Galitski, T. Kitagawa, M. Levin and G. Refael, with whom they began their journey in this field. The authors also thank I. Esin for help with figures and helpful discussions. N.H.L. acknowledges support from the European Research Council (ERC) under the European Union Horizon 2020 Research and Innovation Programme (grant agreement number 639172), and from the Israeli Center of Research Excellence (I-CORE) 'Circle of Light'. M.S.R. gratefully acknowledges the support of the European Research Council (ERC) under the European Union Horizon 2020 Research and Innovation Programme (grant agreement number 678862), the Villum Foundation, and CRC 183 of the Deutsche Forschungsgemeinschaft.

Author contributions
M.S.R. and N.H.L. contributed equally to the organization and writing of this Review.

Competing interests
The authors declare no competing interests.

Peer review information
Nature Reviews Physics thanks the anonymous reviewer(s) for their contribution to the peer review of this work.